

Reliability of DC power grids under uncertainty: a large deviations approach

Tommaso Nesti, Jayakrishnan Nair and Bert Zwart

Abstract

The advent of renewable energy has huge implications for the design and control of power grids. Due to increasing supply-side uncertainty, traditional reliability constraints such as strict bounds on current, voltage and temperature in a transmission line have to be replaced by chance constraints which are computationally hard. In this paper we use large deviations techniques to study the probability of current and temperature overloads in a DC network with stochastic power injections, and develop corresponding safe capacity regions. In particular, we characterize the set of admissible power injections such that the probability of overloading of any line over a given time interval stays below a fixed target. We show how enforcing (stochastic) constraints on temperature, rather than on current, results in a less conservative approach and can thus lead to capacity gains in power grids.

I. INTRODUCTION

The electricity network is one of the backbones of modern society, and is expected to function at all times. The advent of renewable energy sources such as wind and solar generation have put this requirement under pressure due to their considerable intermittency. Both the US and Europe have set long-term goals on the usage of renewable energy, but the effects of the integration of renewable sources into the power grid are already felt today. For example, 80% of the bottlenecks in the European transmission grid are already caused by renewables [1]. Dealing

T. Nesti is with Centrum Wiskunde Informatica (CWI), Science Park 123, Amsterdam, 1098 XG, Netherlands (email: nesti@cwi.nl).

Jayakrishnan Nair is with IIT Bombay, Powai, Mumbai, Maharashtra 400076, India (jayakrishnan.nair@ee.iitb.ac.in).

B. Zwart is with Centrum Wiskunde Informatica (CWI), Science Park 123, Amsterdam, 1098 XG, Netherlands. He also holds professorial positions at Eindhoven University of Technology (email: bert.zwart@cwi.nl).

This research is supported by an NWO VICI grant.

with the uncertainty of renewable generation effectively is therefore an essential requirement in the operation of modern grids.

A well-controlled power grid matches supply and demand at all times, ensuring that line constraints are not violated. The system operator achieves this by making periodic control actions (typically every 5-15 minutes) that adapt the operating point of the grid in response to changing conditions [2]. A key assumption driving grid operation today is that the grid remains roughly static between control instants. In other words, it is assumed that the operating point does not change much between control instants. Thus, the operator simply ensures that line constraints are satisfied at each control instant. This assumption is of course reasonable when there is little short term uncertainty in demand and supply.

However, with increasing penetration of renewable sources, supply-side uncertainty is bound to grow dramatically going forward. Renewable energy sources, like wind and solar, can exhibit considerable variability in power generation in the short term [3], [4]. Consequently, in the near future, system operators will no longer be able to assume that the grid is static between control instants, and will have to set the operating point taking into account its variability in the short-term. This entails setting the operating point of the grid with stochastic guarantees on constraint satisfaction [5], [6]. In other words, the operating point must be set such that line constraint violation is a sufficiently rare event until the next control instant. Moreover, schemes like economic dispatch and Optimal Power Flow (OPF) need to be adapted in such a way that uncertainty is taken into account, and outages stay rare events.

In an optimization framework, this leads to chance constraints which are hard to evaluate analytically. The analysis of such constraints, such as the probability of overheating or a blackout, has so far only been done using rare event simulation techniques [6]–[8]. Although detailed simulations can be more accurate, short-term planning requires tools that enable the grid operator to handle the stochastic constraints much faster. We aim to develop analytic tools, which are explicit enough so as to be useful for planning and control of power grids in the short-term.

The main contribution of this paper is the development of tractable capacity regions for a power grid with variable sources. Specifically, we characterize the set of admissible power injections, such that the overheating of any transmission line in the network over a given interval is a rare event. Our main technique to achieve this is the theory of large deviations. Specifically, we model the random power input sources as small-noise diffusions, for which a comprehensive and sufficiently explicit theory of large deviations is available. We use the popular DC approximation

[9], [10] to model currents on the network. The DC approximation is reasonable if voltages in the network are constant and the voltage angles are small, which is the case for high-voltage networks. This allows us to apply Freidlin-Wentzell theory [11] to approximate the probability of an overflow event in the network, which in turn leads to our capacity region characterization. For the simplest network with two nodes and one line, our results have been published without proof in the extended abstract [12].

Avoiding transmission line overheating is a key reliability constraint in order to avoid sag and loss of tensile strength [13], one of the key causes of the Northeast blackout in 2003 [14] and the San Diego blackout in 2011 [15].

The classical approach for enforcing this constraint is to impose a certain upper bound on each line current. In Section III, we follow this approach and develop capacity regions based on bounding the probability that any line current exceeds its bound over a given interval. We prove an important convexity property of this capacity region, which enables its application in optimization formulations such as OPF. When the random power injections are modeled by an Ornstein-Uhlenbeck (OU) process, we express this capacity region in closed form.

Since line temperature responds gradually to current, a constraint on current is much more conservative than the constraint on temperature. This is because a transient current overload does not necessarily imply an overload in temperature. Thus, imposing a constraint on the probability of current overload results in a smaller capacity region compared to the same constraint on the probability of temperature overload. This observation was noted via simulations in [7]. In Section IV, we show that it is possible to develop large deviations estimates for temperature constraint violations that lead to larger capacity regions, than the ones obtained when only considering currents. However, it turns out that it is hard to compute such temperature-based regions. We overcome this issue by developing two tractable approximations of this capacity region. The first is an inner bound, and the second is based on a Taylor series expansion of the decay rate of the temperature overload probability. Both regions capture the benefits of incorporating the transient relationship between temperature and current. Moreover, both regions have the same computational complexity as the current-based capacity region. For the case of OU power injections, we are able to express these capacity regions in closed form.

There are several related strands of literature, apart from the papers dealing with rare event simulation that have been mentioned above. Much of the literature on power flow in electricity grids considers deterministic settings, focusing on computational and/or optimization issues.

Power flow papers that analyze stochastic models include [5], [13], [16], [17]. One remark about these papers is that they model stochastic behavior at particular snapshots of time, as opposed to the process-level model in this paper. Process-level models have been considered in simulation studies [6], [7] and in recent works on chance-constrained versions of OPF [18], [19]. Our work is complementary to recent efforts on managing supply-side uncertainty via demand response [20], [21], energy storage [22], [23], and market (re)design [24], [25].

The paper is organized as follows. In Section II, we describe our model for power injections, line currents and line temperatures. Sections III and IV constitute the core of the paper: we develop and characterize large deviations-based capacity regions for line currents and line temperatures, respectively, and provide explicit expressions in the particular case that the power injections follow a multivariate Ornstein-Uhlenbeck process. In Section V, numerics for the OU case are presented. We summarize and discuss future directions in Section VI.

II. SYSTEM MODEL

In this section, we describe our model for power injections, line currents, and line temperatures.

The network is specified by a connected, undirected graph $\mathcal{G} = (\mathcal{N}, \mathcal{L})$, where $\mathcal{N} = \{0, 1, 2, \dots, N\}$ is the set of vertices (also called nodes or buses), and $\mathcal{L} = \{1, 2, \dots, L\}$ is the set of edges (also called branches, connections or lines). We have $|\mathcal{N}| = N + 1$ and $|\mathcal{E}| = L$, and connectedness implies $L \geq N$. To define the line currents, we assign the following orientation to \mathcal{G} : the edge $\{i, j\}$ *exits* from node i if $i < j$, and *enters* it otherwise. Under this orientation, we will denote an edge connecting nodes i and j as the ordered pair (i, j) , with $i < j$. Edges will be listed according to lexicographical order.

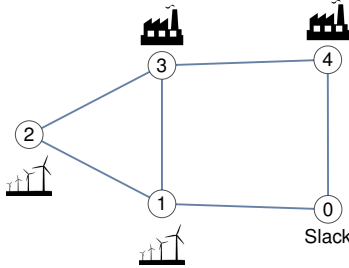


Fig. 1: Example of network with two deterministic and two stochastic power injections. Here $N = 4$, $m = 2$, $\mathcal{L} = \{(0, 1), (0, 4), (1, 2), (1, 3), (2, 3), (3, 4)\}$.

Nodes 1 through N are either sources or sinks, and Node 0 is the slack node, which ensures that there are no active power imbalances in the network. Let vector $S(t) = (S_i(t))_{i \in \mathcal{N}}$ be the vector of active power injections at time t . We assume that power injections at nodes $1, \dots, m \leq N$, are stochastic. This models, for example, buses that are renewable generators. On the other hand, power injections at nodes $m+1, \dots, N$ are deterministic and constant, modeling conventional loads/generators. We will be interested in capturing the probability of current/temperature overload over a finite horizon $[0, T]$, which corresponds to the interval between periodic control actions by the grid operator. In practice, T would be of the order of 10 minutes. Thus, the buses in $\{m+1, \dots, N\}$ are those that may be assumed to have a steady power injection over this time scale. The power injection vector is of the form $S(t) = (S_0(t), X(t), \mu_D)$, where $X(t) \in \mathbb{R}^m$ is the vector of stochastic injections, and $\mu_D = (\mu_{D,i})_{i=m+1}^N \in \mathbb{R}^{N-m}$.

We denote the initial condition for the stochastic power injections by $\mu := X(0)$. Define $\bar{\mu} := (\mu, \mu_D)$. We may interpret $\bar{\mu}$ as the vector of power injections set by the grid operator at time 0. Subsequently, some of the power injections (corresponding to the first m dimensions) fluctuate randomly because of the variability of the renewable generators. In this paper, our focus is to characterize the capacity region of the power grid, i.e. the set of power injection vectors $\bar{\mu}$ such that the probability of current/temperature overload over a finite horizon $[0, T]$ is below a prescribed target p .

In what follows, we first describe the mapping from power injections to line currents under the DC approximation. We then describe the mapping from line currents to line temperatures. Finally, we describe our stochastic diffusion model for the power injections.

A. Line currents under the DC approximation

In this section, we relate the line currents in the power grid to the power injections. Throughout this paper, we make use of the *DC approximation*, which leads to a linear relationship between power injections and line currents. We note that the use of the DC approximation is standard in the literature [9], [10], [26]. The more general AC power flow equations are often analytically intractable, and may not even be well-posed [27]–[29].

Let $I(t) = (I_\ell(t))_{\ell \in \mathcal{L}}$ be the vector of line currents, and $K(t) = (K_\ell(t))_{\ell \in \mathcal{L}}$ be the vector of line temperatures. Each line ℓ in a power grid is associated with a thermal limit $K_{\max, \ell}$, which is the maximum permissible temperature of the line [13]. We define $I_{\max, \ell} > 0$ such that if $|I_\ell(t)| = I_{\max, \ell}$ at all times, then $\lim_{t \rightarrow \infty} K_\ell(t) = K_{\max, \ell}$. Throughout this paper, we work

with *normalized* currents $Y(t) = (Y_\ell(t))_{\ell \in \mathcal{L}}$, defined as $Y_\ell(t) = \frac{I_\ell(t)}{I_{\max, \ell}}$. The traditional approach for ensuring line reliability is to impose the condition $\|Y(t)\|_\infty := \max_{\ell \in \mathcal{L}} |Y_\ell(t)| < 1$ at all times. In this spirit, we characterize the capacity region of the power grid based on bounding the current overload probability in Section III. In other words, we characterize the set of initial power injection vectors $\bar{\mu}$ such that $P(\|Y\| \geq 1) \leq p$, where p is a prescribed reliability target, and $\|f\| := \max_{t \in [0, T]} \|f(t)\|_\infty$ for a continuous function $f : [0, T] \rightarrow \mathbb{R}^L$.

Under the DC approximation, $Y(t)$ is of the form

$$Y(t) = CX(t) + y,$$

where $C \in \mathbb{R}^{L \times m}$ and $y \in \mathbb{R}^L$. In the remainder of this section, we briefly recall the DC approximation and derive the structure of the matrix C and the vector y . For notational simplicity, we suppress the dependence of power, voltage and current on time when not essential.

Let $\beta_{ij} = \beta_{ji} \in \mathbb{R}$ be the susceptance of line $(i, j) \in \mathcal{L}$, with $\beta_{ij} = 0$ if and only if there is no connection between node i and node j . Let $V_j = |V_j|e^{i\theta_j}$ denote the voltage at node j , where V_j is the voltage magnitude and θ_j is the voltage phase. The DC approximation consists of the following assumptions:

- Voltage magnitudes $|V_j|$ are all equal to 1.
- Phase differences between neighboring nodes are small: $\forall (i, j) \in \mathcal{L}, |\theta_i - \theta_j| \ll 1$.
- Resistances are negligible with respect to reactances.

Under these assumptions, the power flow equations read

$$S_i = \sum_{j=1}^{N+1} \beta_{ij}(\theta_i - \theta_j), \quad i = 0, \dots, N \quad (\text{II.1})$$

and the (active) current I_{ij} going from node i to node j is given by

$$I_{ij} = \beta_{ij}(\theta_i - \theta_j), \quad (i, j) \in \mathcal{L}. \quad (\text{II.2})$$

Now, we define:

- the Laplacian matrix $B \in \mathbb{R}^{(N+1) \times (N+1)}$

$$B_{ij} = \begin{cases} -\beta_{ij} & \text{if } i \neq j \\ \sum_{k \neq j} \beta_{ik} & \text{if } i = j \end{cases}$$

- the edge-vertex incidence matrix $A \in \mathbb{R}^{L \times (N+1)}$

$$A_{\ell k} = \begin{cases} 0 & \text{if } \ell = (i, j) \text{ and } k \notin \{i, j\} \\ 1 & \text{if } \ell = (i, j) \text{ and } k = i \\ -1 & \text{if } \ell = (i, j) \text{ and } k = j \end{cases}$$

- the diagonal matrix $D \in \mathbb{R}^{L \times L}$, $D_{\ell\ell} = \beta_{ij} \neq 0$, where $\ell = (i, j)$.

Then equations (II.1) and (II.2) read, in matrix form,

$$S = B\theta, I = DA\theta. \quad (\text{II.3})$$

We now recall some well-known properties of the Laplacian matrix B and the system (II.3), [18].

Lemma II.1. *If the network graph is connected, the Laplacian matrix $B \in \mathbb{R}^{(N+1) \times (N+1)}$ has rank N and the system (II.3) is feasible iff $\sum_{i=1}^{N+1} S_i = 0$. Moreover, if the system is feasible then for any $j \in \{0, \dots, N\}$, there exists a solution with $\theta_j = 0$.*

Note that under the DC approximation, the sum of all active power injections in the network equals zero. Moreover, by Lemma II.1, we may assume without loss of generality that $\theta_0 = 0$. The following construction is inspired by [19]. Let $\hat{B} \in \mathbb{R}^{N \times N}$ be the principal submatrix of B obtained by striking out the first column and row, and for a vector $x \in \mathbb{R}^{N+1} = [x_0, x_1, \dots, x_N]$ let $\hat{x} = [x_1, \dots, x_N]$. Since B has rank N , \hat{B} is nonsingular and, fixing $\theta_0 = 0$, we have

$$B\theta = S \iff \hat{B}\hat{\theta} = \hat{S} \iff \hat{\theta} = \hat{B}^{-1}\hat{S} \iff \theta = \check{B}S, \quad (\text{II.4})$$

where $\check{B} = \begin{pmatrix} 0 & 0 \\ 0 & \hat{B}^{-1} \end{pmatrix}$. By equations (II.3) and (II.4) we obtain that the linear mapping between the power injections $S \in \mathbb{R}^{N+1}$ and the currents $I \in \mathbb{R}^L$ is $I = \tilde{C}S$, where $\tilde{C} := DA\check{B} \in \mathbb{R}^{L \times (N+1)}$. It now follows that $Y(t) = \overline{C}S(t)$, where the matrix \overline{C} has normalized rows as follows: $\overline{C}_{ij} = \frac{\tilde{C}_{ij}}{I_{\max,i}}, i = 1, \dots, L, j = 1, \dots, N+1$.

We can write the dependency of the normalized currents on the stochastic power injections and the deterministic ones more explicitly. To this end, notice that due to the structure of \check{B} we have that the first column of \overline{C} is zero, yielding that \overline{C} is of the form $\overline{C} = [\mathbf{0} | C | C_D]$, where $\mathbf{0} = [0, \dots, 0]^T \in \mathbb{R}^L$, C is the $L \times m$ submatrix of \overline{C} constituted of columns 2 to $m+1$ and C_D is the $L \times (N-m)$ submatrix of \overline{C} constituted of columns $m+2$ to $N+1$. With this notation,

we have

$$Y(t) = \overline{C}S(t) = \left[\begin{array}{c|c|c} \mathbf{0} & C & C_D \end{array} \right] \begin{bmatrix} S_0(t) \\ X(t) \\ \mu_D \end{bmatrix},$$

i.e.,

$$Y(t) = CX(t) + y, \quad (\text{II.5})$$

where $y := C_D\mu_D$. We will refer to equation (II.5) as the DC power flow equation. Note that the initial condition for the normalized currents is given by $Y(0) = \nu$, where $\nu := C\mu + y$. In what follows we always suppose that $\|\nu\| < 1$, i.e. at time $t = 0$ the current is below the critical level.

The following lemma shows that matrix C in (II.5) has rank m , i.e. the number of stochastic power injections.

Lemma II.2. *If the network graph is connected, $\text{rank}(\overline{C}) = N$ and $\text{rank}(C) = m$. In particular, the matrix C has linearly independent columns.*

The proof of Lemma II.2 can be found in Appendix A.

B. Mapping between line current and line temperature

In this section, we describe how line temperature depends on line current. Recall that $K_\ell(t)$ denotes the temperature of line ℓ . We work with *normalized* line temperatures, defined as follows. Let $K_{\text{env},\ell}^e$ be the ambient temperature around line ℓ . We define the normalized line temperatures $\Theta(t) = (\Theta_\ell(t))_{\ell \in \mathcal{L}}$ as $\Theta_\ell(t) = \frac{K_\ell(t) - K_{\text{env},\ell}^e}{K_{\text{max},\ell} - K_{\text{env},\ell}^e}$. Note that the reliability constraint on line temperatures reads $\|\Theta\|_\infty < 1$. In this spirit, in Section IV, we characterize the capacity region of the power grid based on bounding the temperature overload probability. In other words, we characterize the set of initial power injection vectors $\bar{\mu}$ such that $P(\|\Theta\| \geq 1) \leq p$, where p is a prescribed reliability target.

The transient relationship between the normalized temperature Θ_ℓ and the normalized current is given by the ordinary differential equation [30]

$$\tau_\ell \frac{d\Theta_\ell}{dt} + \Theta_\ell = (Y_\ell)^2, \quad (\text{II.6})$$

where $\tau_\ell > 0$ denotes the thermal time constant of the transmission line l . Thus, we have

$$\Theta_\ell(t) = \Theta_\ell(0)e^{-t/\tau_\ell} + \frac{1}{\tau_\ell} \int_0^t e^{-(t-s)/\tau_\ell} (Y_\ell(s))^2 ds. \quad (\text{II.7})$$

Note that the instantaneous line temperature depends on the history of the line current process, with an exponentially decaying weight on past values. The parameter τ_ℓ determines the dependence of the instantaneous temperature on past values of current. Thus, if τ_ℓ is small, the dependence on past current values becomes weaker, i.e., the line temperature responds more quickly to changes in current. In the limit as $\tau_\ell \downarrow 0$, line temperature responds instantaneously to current, i.e., $\Theta_\ell(t) = (Y_\ell(t))^2$.

For simplicity, we assume the initial condition $\Theta_\ell(0) = (Y_\ell(0))^2 = \nu_\ell^2 \quad \forall \ell \in \mathcal{L}$ for line temperatures. Note that ν_ℓ^2 is the steady state temperature corresponding to a constant line current ν_ℓ .

With the above initial condition, let us denote the mapping from the current process Y to the temperature process Θ as $\Theta = \xi_\tau(Y)$, where we emphasize the dependence on the thermal time constants $\tau = (\tau_l)_{l \in \mathcal{L}}$.

C. Model for power injections

In this section, we describe our stochastic model for the power injections $X(t)$. Recall that in order to characterize the capacity region of the power grid, we have to estimate the following overload probabilities:

$$P(\|Y\| \geq 1), \quad P(\|\Theta\| \geq 1).$$

We use the theory of large deviations to estimate these probabilities. Accordingly, in the standard manner (see [11]), for $\epsilon > 0$ we define the ϵ -scaled power injection processes $X_i^\epsilon(t)$ as the strong solution of the 1-dimensional stochastic differential equation (SDE)

$$dX_i^\epsilon(t) = b_i(X_i^\epsilon(t))dt + \sqrt{\epsilon}l_i(X_i^\epsilon(t))dW_i(t),$$

with initial condition $X_i^\epsilon(0) = \mu_i$, for $i = 1, \dots, m$.

The parameter $\epsilon > 0$ captures the amount of randomness in the power injections. For all $i = 1, \dots, m$ we make the following assumptions:

- $b_i : \mathbb{R} \rightarrow \mathbb{R}$ is Lipschitz continuous, differentiable and such that $b_i(\mu_i) = 0$;
- $l_i : \mathbb{R} \rightarrow (0, \infty)$ is Lipschitz continuous, bounded and differentiable;
- $W_i(t)$ is a standard Brownian motion in \mathbb{R} .

The process $X^\epsilon(t) = (X_1^\epsilon(t), \dots, X_m^\epsilon(t))$ is the strong solution of the m -dimensional SDE

$$dX^\epsilon(t) = b(X^\epsilon(t))dt + \sqrt{\epsilon}L(X^\epsilon(t))dW(t), \tag{II.8}$$

with $X^\epsilon(0) = \mu$, $b(x) = (b_1(x_1), \dots, b_m(x_m))$, $L(x) = \text{diag}((l_i(x_i))_{i=1, \dots, m})$ and $W(t) = (W_i(t))_{i=1, \dots, m}$.

The ϵ -scaled current process $Y^\epsilon(t) = (Y^\epsilon)_{\ell \in \mathcal{L}}$ is defined as per the DC power flow equations: $Y^\epsilon(t) = CX^\epsilon(t) + y$. Similarly, the ϵ -scaled temperature process $\Theta_\tau^\epsilon(t) = (\Theta_\tau^\epsilon)_{\ell \in \mathcal{L}}$, with thermal constant τ , is defined as $\Theta_\tau^\epsilon = \xi_\tau(Y^\epsilon)$. In the following sections, we apply the theory of large deviations to estimate the probabilities

$$P(\|Y^\epsilon\| \geq 1), \quad P(\|\Theta^\epsilon\| \geq 1),$$

in the limit as $\epsilon \downarrow 0$.

III. CAPACITY REGIONS CHARACTERIZATION BASED ON CURRENT OVERLOAD

In this section, we characterize the capacity region of the power grid obtained by bounding the probability of current overload over a finite horizon. Specifically, we use large deviations techniques to approximate the set of (initial) power injections such that the probability of current overload (on any line) over the interval $[0, T]$ is bounded from above by a pre-defined threshold. Recall that we interpret T as the interval between control actions by the grid operator. Our focus therefore is to characterize the space of initial power injections that can be ‘set’ by the grid operator at time 0, such that the probability that the inherent variability in the stochastic sources leads to a current overload before the next control instant is small.

The above approach is in line with the conventional technique of enforcing the thermal limits of the transmission lines by capping the peak current on each line. Note that this approach is conservative, in that it ignores the transient relationship between line current and line temperature: a short-lived current overload may not lead to a temperature overload. Indeed, as we show in Section IV-A, the capacity region of the power grid gets enlarged when we explicitly take the transient relationship between line current and line temperature into account.

In the following, we first characterize the large deviations decay rate corresponding to the current overflow event $\{\|Y^\epsilon\| \geq 1\}$ in the limit as $\epsilon \downarrow 0$. Next, we use this characterization to define the current-overload based capacity region of the power grid. We then prove a convexity result for this capacity region, which facilitates its application as a constraint in OPF. We also prove two lemmas that are useful for computing the capacity region in practice. Finally, we give a closed-form characterization of the capacity region when the stochastic injections follow an Ornstein-Uhlenbeck process.

A. Large deviations decay rate for current overload

In this section, we characterize the large deviations decay rate corresponding to the current overload event $\{\|Y^\epsilon\| \geq 1\}$. Our analysis is based on the Freidlin-Wentzell theory (see section 5.6 in [11]).

The power injections process X^ϵ satisfies the hypothesis of Theorem 5.6.7 of [11], and thus it satisfies a sample path large deviations principle (SPLDP) over $C_\mu([0, T]) = \{g : [0, T] \rightarrow \mathbb{R}^m : g \text{ is continuous and } g(0) = \mu\}$, with good rate function

$$\mathcal{I}_p(g) = \sum_{i=1}^m \mathcal{I}_{p,i}(g_i). \quad (\text{III.1})$$

Here, $g = (g_1, \dots, g_m)$ and $\mathcal{I}_{p,i}$ is the good rate function for the SPLDP associated with the process $X_i^\epsilon(t)$, $i = 1, \dots, m$, and it is given by

$$\mathcal{I}_{p,i}(g_i) = \begin{cases} \frac{1}{2} \int_0^T \left(\frac{g'_i - b_i(g_i)}{l_i(g_i)} \right)^2 dt & \text{if } g_i \in H_{\mu_i}^1(\mathbb{R}), \\ \infty & \text{if } g_i \in H_{\mu_i}^1(\mathbb{R}). \end{cases}$$

Here $H_\mu^1(\mathbb{R}^m) := \{g : [0, T] \rightarrow \mathbb{R}^m : g(t) = \mu + \int_0^t \phi(s) ds, \phi \in L_2([0, T])\}$ is the space of absolutely continuous functions with value μ at 0 and which possess a square integrable derivative.

Recall that the relationship between the current and power injections processes is given by the DC power flow equations (II.5). Thanks to the Contraction Principle ([11], Theorem 4.2.1), the current process Y^ϵ satisfies a SPLDP with good rate function

$$\mathcal{I}_c(f) = \inf_{\substack{g \in H_\mu^1 \\ y + Cg = f}} \mathcal{I}_p(g).$$

Thanks to Lemma II.2, the matrix C has linear independent columns. Therefore, its Moore-Penrose inverse has an explicit formula $C^+ = (C^T C)^{-1} C^T$ and it is a left inverse of C . Thus, for $f \in y + C(H_\mu^1(\mathbb{R}^m)) \subset H_\nu^1(\mathbb{R}^L)$ the equation $y + Cg = f$ has unique solution $g = C^+(f - y)$, so that

$$\mathcal{I}_c(f) = \begin{cases} \mathcal{I}_p(C^+(f - y)) & \text{if } f \in y + C(H_\mu^1(\mathbb{R}^m)), \\ \infty & \text{otherwise.} \end{cases} \quad (\text{III.2})$$

For the current overload event we then have that

$$\limsup_{\epsilon \rightarrow 0} \epsilon \log \mathbb{P}(\|Y^\epsilon\| \geq 1) \leq -\mathcal{I}_c^*, \quad (\text{III.3})$$

with

$$\mathcal{I}_c^* = \inf_{\substack{f \in y + CH_\mu^1: \\ \|f\| \geq 1}} \mathcal{I}_c(f) = \inf_{\substack{g \in H_\mu^1: \\ \|y + Cg\| \geq 1}} \mathcal{I}_p(g) \quad (\text{III.4})$$

the *decay rate* corresponding to the current overload event. Note that $\mathcal{I}_c^* = \inf_{\substack{f \in y + CH_\mu^1: \\ \|f\| \geq 1}} \mathcal{I}_c(f) = \inf_{\substack{f \in H_\nu^1: \\ \|f\| \geq 1}} \mathcal{I}_c(f)$, because if $f \in H_\nu^1 \setminus (y + CH_\mu^1)$, then $\mathcal{I}_c(f) = \infty$.

B. Capacity region based on current overload

Equation (III.3) yields the following approximation for the current overload probability for small ϵ :

$$\mathbb{P}(\|Y^\epsilon\| \geq 1) \approx e^{-\mathcal{I}_c^*(\bar{\mu})/\epsilon}. \quad (\text{III.5})$$

We use the above approximation to define the following capacity region for the power grid, based on the constraint that the probability of current overflow must not exceed p , where $p > 0$ is a small pre-defined threshold.

$$\tilde{\mathcal{R}}_{\epsilon,p}^{(c)} := \{\bar{\mu} \in \mathbb{R}^N : \mathcal{I}_c^*(\bar{\mu}) \geq -\epsilon \log(p)\}. \quad (\text{III.6})$$

In the remainder of this section, we shed light on structural properties and computational aspects of this capacity region. Our first result shows that the capacity region is convex with respect to the deterministic power injections.

Lemma III.1. $\tilde{\mathcal{R}}_{\epsilon,p}^{(c)}$ is convex in the deterministic power injections vector μ_D .

Proof. First notice that a vector (μ, μ_D) such that $\|\nu\| = \|C\mu + C_D\mu_D\| < 1$ belongs to the capacity region $\tilde{\mathcal{R}}_{\epsilon,p}^{(c)}$, i.e.

$$\mathcal{I}_c^*(\mu, \mu_D) = \inf_{\substack{g \in H_\mu^1: \\ \|C_D\mu_D + Cg\| = 1}} \mathcal{I}_p(g) \geq \epsilon \log(1/p),$$

if and only if the following implication holds:

$$\exists g \in H_\mu^1 \text{ s.t. } \mathcal{I}_p(g) < \epsilon \log(1/p) \implies \|C_D\mu_D + Cg\| < 1. \quad (\text{III.7})$$

Consider two admissible vectors $(\mu, \mu_D), (\mu, \tilde{\mu}_D) \in \tilde{\mathcal{R}}_{\epsilon,p}^{(c)}$, and let $\lambda \in [0, 1]$. We want to show that $(\mu, \lambda\mu_D + (1 - \lambda)\tilde{\mu}_D) \in \tilde{\mathcal{R}}_{\epsilon,p}^{(c)}$. Let $g \in H_\mu^1$ be such that $\mathcal{I}_p(g) < \epsilon \log(1/p)$. Thus $\|\lambda C_D\mu_D + (1 - \lambda)C_D\tilde{\mu}_D + Cg\| = \|\lambda(C_D\mu_D + Cg) + (1 - \lambda)(C_D\tilde{\mu}_D + Cg)\| \leq \lambda\|(C_D\mu_D + Cg)\| + (1 - \lambda)\|(C_D\tilde{\mu}_D + Cg)\| < \lambda + (1 - \lambda) = 1$, where we used property (III.7) and the fact that $(\mu, \mu_D), (\mu, \tilde{\mu}_D)$ are admissible. Therefore, $\lambda\mu_D + (1 - \lambda)\tilde{\mu}_D$ is admissible (notice that the above calculation implies in particular that $\|C\mu + C_D(\lambda\mu_D + (1 - \lambda)\tilde{\mu}_D)\| < 1$). \square

Lemma III.1 is important as convexity enables the set of allowable deterministic injections to be incorporated as a constraint in OPF problems (see, for example, [19]). For the special case where power injections are modeled as an Ornstein Uhlenbeck process, we show in Section III-C that the capacity region $\tilde{\mathcal{R}}_{\epsilon,p}^{(c)}$ itself is convex.

Next, we note that the decay rate \mathcal{I}_c^* is the minimum of the decay rates corresponding to the overload event for each link. Letting

$$\psi_\ell = \inf_{\substack{f \in H_\nu^1: \\ \|f_\ell\|_\infty \geq 1}} \mathcal{I}_c(f) = \inf_{\substack{g \in H_\mu^1: \\ \|y_\ell + C_\ell g\|_\infty \geq 1}} \mathcal{I}_p(g),$$

with C_ℓ being the ℓ -th row of matrix C , we see that $\mathcal{I}_c^* = \min_{\ell \in \mathcal{L}} \psi_\ell$. In other words, the decay rate for current overload in the network is simply the decay rate corresponding to overload on the link most likely to overload. Observe that if $C_\ell = 0$, then $Y_\ell^\epsilon(t) = Y_\ell^\epsilon(0) = y_\ell$ is constant and does not depend on the stochastic power injections. In particular, since $\|y_\ell\| = \|\nu_\ell\| < 1$, we have $\psi_\ell = \inf_{\substack{g \in H_\mu^1: \\ \|y_\ell\|_\infty \geq 1}} \mathcal{I}_p(g) = \infty$. Therefore we have $\mathcal{I}_c^* = \min_{\ell \in \mathcal{L}'} \psi_\ell$, where $\mathcal{L}' := \{\ell \in \mathcal{L} : C_\ell \neq 0\}$.

The next lemma shows that the current overload on any link most likely occurs at the end time T .

Lemma III.2. *For any $\ell \in \mathcal{L}'$, $\psi_\ell = \inf_{\substack{g \in H_\mu^1: \\ |y_\ell + C_\ell g(T)|=1}} \mathcal{I}_p(g)$.*

The proof of this lemma is provided in Section VII. For $a \neq \nu_\ell$, define

$$\psi_\ell^{(a)} = \inf_{\substack{f \in y + CH_\mu^1: \\ f_\ell(T)=a}} \mathcal{I}_p(f) = \inf_{\substack{g \in H_\mu^1: \\ y_\ell + C_\ell g(T)=a}} \mathcal{I}_p(g),$$

so that $\psi_\ell = \psi_\ell^{(1)} \wedge \psi_\ell^{(-1)}$ and

$$\mathcal{I}_c^* = \min_{\ell \in \mathcal{L}'} \psi_\ell^{(1)} \wedge \psi_\ell^{(-1)}, \quad (\text{III.8})$$

where $a \wedge b = \min\{a, b\}$. The following lemma, also proved in Section VII, will be useful later.

Lemma III.3. *The function $a \rightarrow \psi_\ell^{(a)}$ is non-decreasing for $a > \nu_\ell$ and non-increasing for $a < \nu_\ell$.*

Note that (III.8) allows us to rewrite the capacity region as follows.

$$\tilde{\mathcal{R}}_{\epsilon,p}^{(c)} = \bigcap_{\substack{\ell \in \mathcal{L}' \\ a \in \{-1, 1\}}} \{\bar{\mu} \in \mathbb{R}^N : \psi_\ell^{(a)} \geq -\epsilon \log(p)\}.$$

Thus, obtaining the capacity region $\tilde{\mathcal{R}}_{\epsilon,p}^{(c)}$ hinges on computing $\psi_\ell^{(a)}$, which by definition is the

solution of the variational problem

$$\inf_{\substack{x \in H_\mu^1: \\ y_\ell + C_\ell x(T) = a}} \mathcal{I}_p(x).$$

To solve this variational problem with boundary constraints, one can employ the Euler-Lagrange equation.

For simple diffusion models, this approach can be used to obtain the optimal path and $\psi_\ell^{(a)}$ in closed form, leading to an explicit characterization of the capacity region $\tilde{\mathcal{R}}_{\epsilon,p}^{(c)}$. In the following, we illustrate this for the case where the power injections are modeled as an Ornstein-Uhlenbeck process.

C. Explicit computations for Ornstein-Uhlenbeck process

In this section we suppose that the power injections process $X^\epsilon(t)$ is a multivariate Ornstein-Uhlenbeck (OU) process, of the form

$$dX^\epsilon(t) = D(\mu - X^\epsilon(t))dt + \sqrt{\epsilon}LdW(t) \quad (\text{III.9})$$

i.e. the functions $b(\cdot)$ and $L(\cdot)$ in the SDE (II.8) are

$$b(x) = D(\mu - x), \quad L(x) = L$$

where $D = \text{diag}(\gamma_1, \dots, \gamma_m)$ and $L = \text{diag}(l_1, \dots, l_m)$ are diagonal matrices, and $\gamma_i, l_i > 0$ for all $i = 1, \dots, m$. For this model, the capacity region can be expressed in closed form.

In [31] the optimal current paths and values are obtained for a single line and a deterministic initial value $y = 0 \in \mathbb{R}$. Since our focus is on capacity regions, in our setting we need to consider a general vector $y \in \mathbb{R}^L$ of deterministic initial values for the currents. As before, let C_ℓ denote the ℓ -th row of matrix C . Following the methods in [31], for lines $\ell \in \mathcal{L}'$, it can be shown that

$$\psi_\ell^{(a)} = \frac{(a - \nu_\ell)^2}{C_\ell M_T C_\ell^T}, \quad (\text{III.10})$$

where

$$M_t = L^2 D^{-1} (I - e^{-2Dt}) e^{D(t-T)}. \quad (\text{III.11})$$

The corresponding optimal paths for power injections and currents are

$$\begin{aligned} X^{(\ell)}(t) &= (a - \nu_\ell) \frac{M_t C_\ell^T}{C_\ell M_T C_\ell^T} + \mu, \\ Y^{(\ell)}(t) &= C X^{(\ell)}(t) + y. \end{aligned} \quad (\text{III.12})$$

Note that $X^{(\ell)}(t)$ and $Y^{(\ell)}(t)$ are the multidimensional paths: the superscript (ℓ) specifies that these are the optimal path to overload in line ℓ . It follows easily that

$$\mathcal{I}_c^*(\bar{\mu}) = \min_{\ell \in \mathcal{L}'} \frac{(1 - |\nu_\ell|)^2}{C_\ell M_T C_\ell^T}.$$

We therefore have the following result.

Proposition III.1. *If $X^\epsilon(t)$ is defined by (III.9), then*

$$\tilde{\mathcal{R}}_{\epsilon,p}^{(c)} = \bigcap_{\ell \in \mathcal{L}'} \left\{ \bar{\mu} \in \mathbb{R}^N : |\nu_\ell| \leq 1 - \sqrt{\epsilon \log(1/p) C_\ell M_T C_\ell^T} \right\}, \quad (\text{III.13})$$

where $M_t = L^2 D^{-1} (I - e^{-2Dt}) e^{D(t-T)}$. In the particular case when $D = \gamma I$, the capacity region can be rewritten as

$$\tilde{\mathcal{R}}_{\epsilon,p}^{(c)} = \bigcap_{\ell \in \mathcal{L}'} \left\{ \bar{\mu} \in \mathbb{R}^N : |\nu_\ell| \leq 1 - \beta_\ell \right\}, \quad (\text{III.14})$$

where $\beta_\ell := \sqrt{\frac{(1-e^{-2\gamma T})\epsilon \log(1/p)\sigma_\ell^2}{\gamma}}$ and $\sigma_\ell^2 := C_\ell L^2 C_\ell^T = \|LC_\ell^T\|^2$.

Recall that $\bar{\mu} = [\mu_0, \mu, \mu_D]$ and $\nu = C\mu + C_D\mu_D$. From (III.13) we can observe that $\tilde{\mathcal{R}}_{\epsilon,p}^{(c)}$ is a closed convex set; in particular, it is a polyhedron in \mathbb{R}^N . Note that this property enables us to incorporate the capacity region in OPF problems. We make the following remarks based on the above calculations.

- 1) In the case $D = \gamma I$, β_ℓ is a strictly decreasing function of γ . This means that as γ becomes smaller, the capacity region shrinks. This is intuitive, since for small values of γ , the OU process will revert to its long-term mean μ (i.e., the initial condition for which we have stability) with less force.
- 2) As the time between the two control instants T increases, the decay rate $\mathcal{I}_c^*(\bar{\mu})$ becomes smaller, resulting in a smaller capacity region. Intuitively, the longer the time between two control instants, the greater the probability that the fluctuations in the power injections will result in an overload.
- 3) The current decay rate $\mathcal{I}_c^*(\bar{\mu})$ and the corresponding line at most risk of overload $\ell^*(\bar{\mu}) := \arg \min_{\ell \in \mathcal{L}'} \frac{(1-|\nu_\ell|)^2}{C_\ell M_T C_\ell^T}$ depend in an obvious way on the initial current values ν_ℓ and in a non-trivial way on the matrices C, L, D , which enclose information about the topology of the network, the characteristics of the transmission lines and the evolution of the stochastic power injections.

IV. CAPACITY REGIONS CHARACTERIZATION BASED ON TEMPERATURE OVERLOAD

Avoiding overheating of transmission lines is a key reliability constraint for grid operation, in order to avoid sag and loss of tensile strength [13]. In this section, we develop capacity regions for a power grid based on bounding the probability of temperature overload on any transmission, over a finite horizon. These regions are larger than the capacity region developed in Section III-B, which was based on bounding the probability of a current overload on any line.

Since temperature responds gradually to current, a current overload of a short duration does not necessarily imply an overload in temperature. As a result, it is not surprising that we can enlarge the capacity region of the power grid by explicitly capturing the transient relationship between temperature and current, as compared to the conservative approach of bounding line currents. This observation was noted via simulations in [7]. To the best of our knowledge, this paper provides the first analytical treatment of this phenomenon.

In the following, we first characterize the large deviations decay rate corresponding to $P(\|\Theta^{\epsilon,\tau}\|_{\infty} \geq 1)$. Using this decay rate, we define the temperature-overload based capacity region of the power grid. We prove a convexity result for this region, analogous to the result in Section IV. However, due to the highly non-linear relationship between current and temperature, it turns out that the above decay rate is hard to compute explicitly. As a result, the capacity region cannot be expressed in closed form for even the simplest diffusion models (like OU). To address this issue, we develop two approximations of the capacity region. The first is an inner bound, based on a lower bound on the decay rate. The second approximation is based on a first order Taylor expansion of decay rate around $\tau = 0$. These approximations have the following appealing properties, which make them amenable to application in OPF formulations. Firstly, both approximations are supersets of the capacity region $\tilde{\mathcal{R}}_{\epsilon,p}^{(c)}$ based on current overload. Secondly, they have the same computational complexity as $\tilde{\mathcal{R}}_{\epsilon,p}^{(c)}$. Indeed, for the special case where the stochastic power injections are modeled by an OU process, both regions can be expressed in closed form. Finally, both approximations are convex over the deterministic (i.e., controllable) power injections.

A. Capacity region based on temperature overload

In this section, we define the capacity region of the power grid based on bounding the probability of temperature overload on any transmission line. Thanks to the relationship (II.6),

applying the contraction principle yields that $\Theta_{\epsilon,\tau}$ satisfies a SPLDP with good rate function

$$\mathcal{I}_{t,\tau}(h) = \inf_{\substack{f \in H_\nu^1: \\ \xi_\tau(f)=h}} \mathcal{I}_c(f) = \inf_{\substack{f \in y + CH_\mu^1: \\ \xi_\tau(f)=h}} \mathcal{I}_c(f). \quad (\text{IV.1})$$

For the temperature overload event we thus have

$$\limsup_{\epsilon \rightarrow 0} \epsilon \log P(\|\Theta^{\epsilon,\tau}\|_\infty \geq 1) \leq -\mathcal{I}_{t,\tau}^*, \quad (\text{IV.2})$$

where

$$\mathcal{I}_{t,\tau}^* = \inf_{\substack{h \in \xi_\tau(H_\nu^1) \\ \|h\| \geq 1}} \mathcal{I}_{t,\tau}(h) \quad (\text{IV.3})$$

is the *temperature decay rate*. Letting, for $\ell \in \mathcal{L}'$,

$$\omega_\ell = \inf_{\substack{h \in \xi_\tau(H_\nu^1): \\ \|h_\ell\| \geq 1}} \mathcal{I}_{t,\tau}(h) = \inf_{\substack{g \in H_\mu^1: \\ \|\xi_{\tau_\ell}(y_\ell + C_\ell g)\| \geq 1}} \mathcal{I}_p(g),$$

we see that the decay rate for the temperature is $\mathcal{I}_{t,\tau}^* = \min_{\ell \in \mathcal{L}'} \omega_\ell$.

Note that ω_ℓ and $\mathcal{I}_{t,\tau}^*$ depend on $\bar{\mu}$, τ and T . As before, Equation (IV.2) yields the following approximation for the rare event probability:

$$\mathbb{P}(B_{\tau,\epsilon,\bar{\mu}}) \approx e^{-\mathcal{I}_{t,\tau}^*(\bar{\mu})/\epsilon}, \quad \text{for small } \epsilon. \quad (\text{IV.4})$$

This leads to the following definition of the capacity region

$$\begin{aligned} \tilde{\mathcal{R}}_{\tau,\epsilon,p}^{(t)} &:= \{\bar{\mu} \in \mathbb{R}^N : \mathcal{I}_{t,\tau}^*(\bar{\mu}) > -\epsilon \log(p)\} \\ &= \bigcap_{\ell \in \mathcal{L}'} \{\bar{\mu} \in \mathbb{R}^N : \omega_\ell(\bar{\mu}) > -\epsilon \log(p)\}. \end{aligned} \quad (\text{IV.5})$$

We have the following convexity result, which is proved in Section VII.

Lemma IV.1. $\tilde{\mathcal{R}}_{\epsilon,p}^{(t,\tau)}$ is convex in the deterministic power injections vector μ_D .

The variational problem for the temperature overload (IV.3) is difficult to solve in general, and numerics can also prove to be challenging. In the numerics section we will address the computational issues in solving (IV.3) for the simple case of a single line network and OU process for the power injections. As a result, the capacity region $\tilde{\mathcal{R}}_{\tau,\epsilon,p}^{(t)}$ is difficult to work with, even in the simplest settings. Motivated by this difficulty, in the following, we focus on developing approximations for the temperature decay rate and the corresponding capacity regions.

B. Inner bound for the capacity region

In this section, we develop an inner bound for the capacity region $\tilde{\mathcal{R}}_{\tau,\epsilon,p}^{(t)}$. This inner bound is larger than the capacity region $\tilde{\mathcal{R}}_{\epsilon,p}^{(c)}$ based on current overload, and thus captures some of the

benefit of incorporating temperature dynamics into capacity region characterization. Moreover, the inner bound is convex over the deterministic power injections, and has the same computational complexity as the current-based capacity region.

The following lemma provides a lower bound for the temperature decay rate $\mathcal{I}_{t,\tau}^*$.

Lemma IV.2. *For all $\ell \in \mathcal{L}'$, we have*

$$\omega_\ell \geq \psi_\ell^{(\alpha_\ell)} \wedge \psi_\ell^{(-\alpha_\ell)},$$

where

$$\alpha_\ell = \sqrt{\frac{1 - \nu_\ell^2 e^{-T/\tau_\ell}}{1 - e^{-T/\tau_\ell}}}.$$

The proof is given in Section VII. Defining

$$\mathcal{I}_{t,\tau}^{(LB)} := \min_{\ell \in \mathcal{L}'} \psi_\ell^{(\alpha_\ell)} \wedge \psi_\ell^{(-\alpha_\ell)},$$

we see that $\mathcal{I}_{t,\tau}^{(LB)} \leq \mathcal{I}_{t,\tau}^*$. The capacity region based on the lower bound $\mathcal{I}_{t,\tau}^{(LB)}$ is thus

$$\begin{aligned} \tilde{\mathcal{R}}_{\epsilon,p}^{(t,\tau,LB)} &:= \{\bar{\mu} \in \mathbb{R}^N : \mathcal{I}_{t,\tau}^{(LB)}(\tau, \bar{\mu}) \geq -\epsilon \log(p)\} \\ &= \bigcap_{\ell \in \mathcal{L}'} \{\bar{\mu} \in \mathbb{R}^N : \psi_\ell^{(\alpha_\ell)} \wedge \psi_\ell^{(-\alpha_\ell)} \geq -\epsilon \log(p)\} \end{aligned} \quad (\text{IV.6})$$

Note that computing the above region boils down to evaluating $\psi_\ell^{(\cdot)}$. The following proposition summarizes the relation between the above capacity region and the regions based on current and temperature overload.

Proposition IV.1. $\mathcal{I}_c^* \leq \mathcal{I}_{t,\tau}^{(LB)} \leq \mathcal{I}_{t,\tau}^*$ and $\tilde{\mathcal{R}}_{\epsilon,p}^{(c)} \subseteq \tilde{\mathcal{R}}_{\epsilon,p}^{(t,\tau,LB)} \subseteq \tilde{\mathcal{R}}_{\epsilon,p}^{(t)}$ for all $\tau \geq 0$.

Proof. Thanks to Lemma IV.2 we have immediately get that $\mathcal{I}_{t,\tau}^{(LB)}$ is a lower bound for the temperature decay rate, i.e. $\mathcal{I}_{t,\tau}^* \geq \mathcal{I}_{t,\tau}^{(LB)}$. Since $\alpha_\ell > 1 > |\nu_\ell| \forall \ell$, Lemma III.3 implies

$$\psi_\ell^{(\alpha_\ell)} \wedge \psi_\ell^{(-\alpha_\ell)} \geq \psi_\ell^{(1)} \wedge \psi_\ell^{(-1)},$$

yielding that $\mathcal{I}_{t,\tau}^{(LB)} \geq \mathcal{I}_c^*$. □

Proposition IV.1 states that the capacity region based on the lower bound on the temperature decay rate, while being more conservative than the actual temperature-based capacity region, is less conservative than the current-based capacity constraint. Therefore, employing $\tilde{\mathcal{R}}_{\epsilon,p}^{(t,\tau,LB)}$ rather than $\tilde{\mathcal{R}}_{\epsilon,p}^{(c)}$ allows for larger power injections values (i.e., less curtailment) while still being within the (harder to compute) capacity region based on temperature overload. Finally, we note that the inner bound satisfies the following convexity property.

Lemma IV.3. $\tilde{\mathcal{R}}_{\epsilon,p}^{(t,\tau,LB)}$ is convex in the deterministic power injections vector μ_D .

The proof goes along the same lines of the proofs of Lemmas III.1 and IV.1.

C. Taylor approximation of the decay rate and corresponding capacity regions

In this section we derive a heuristic approximation for the temperature decay rate

$$I_{t,\tau}^* = \inf_{\substack{h \in \xi_\tau(y + CH_\mu^1) \\ \|h\| \geq 1}} \mathcal{I}_{t,\tau}(h). \quad (\text{IV.7})$$

Since $\xi_\tau(f) = h$ if and only if $\tau h' + h = f^2$, the temperature rate function (IV.1) can be written as

$$\mathcal{I}_{t,\tau}(h) = \mathcal{I}_{c^2}(\tau h' + h) = \mathcal{I}_c(f_{\tau h' + h}) = \mathcal{I}_p(C^+(f_{\tau h' + h} - y)),$$

where

$$\mathcal{I}_{c^2}(F) = \inf_{\substack{f \in H_\nu^1 \\ f^2 = F}} \mathcal{I}_c(f) \quad (\text{IV.8})$$

is the rate function for the current squared process $(Y^\epsilon(t))^2$ and $f_F := \arg \min_{f \in H_\nu^1, f^2 = F} \mathcal{I}_c(f)$. More explicitly,

$$\mathcal{I}_{t,\tau}(h) = \begin{cases} G(\tau, h) & \text{if } h \in \xi_\tau(y + CH_\mu^1), \\ \infty & \text{otherwise,} \end{cases}$$

with

$$G(\tau, h) := \frac{1}{2} \sum_{i=1}^m \int_0^T \left[\frac{C_i^+ f_{\tau h' + h}(s)' - b_i(C_i^+(f_{\tau h' + h}(s) - y))}{l_i(C_i^+(f_{\tau h' + h}(s) - y))} \right]^2 ds.$$

Taylor approximation 1. Let f_* be the optimal current path to overflow. We will use the approximation

$$\mathcal{I}_{t,\tau}^* \approx \mathcal{I}_{t,\tau}^{(TL)} := \mathcal{I}_c^* + \tau \cdot \nabla_\tau G(\tau, f_*^2)|_{\tau=0}. \quad (\text{IV.9})$$

If τ is of the form $\tau = \tau_0(1, \dots, 1)^T$, $\tau_0 > 0$, we obtain the closed-form expression

$$\mathcal{I}_{t,\tau}^{(TL)} = \mathcal{I}_c^* + \tau_0 \Phi_{f_*} \quad (\text{IV.10})$$

where

$$\Phi_{f_*} := \sum_{i=1}^m \left[K_i(f_*(T), f'_*(T)) - K_i(f_*(0), f'_*(0)) \right], \quad (\text{IV.11})$$

$$K_i(f_*(t), f'_*(t)) := \frac{1}{2} \left(\frac{C_i^+ f'_*(t) - b_i(C_i^+(f_*(t) - y))}{l_i(C_i^+(f_*(t) - y))} \right)^2. \quad (\text{IV.12})$$

In particular the approximation $\mathcal{I}_{t,\tau}^{(TL)}$ depends only on the current decay rate \mathcal{I}_c^* and on the values $f_*(0), (f_*)'(0), f_*(T), (f_*)'(T)$.

The heuristic is motivated by the formal Taylor expansion of $I_{t,\tau}^*$ around $\tau = 0$,

$$\mathcal{I}_{t,0}^* + \tau \cdot \nabla_\tau I_{t,\tau}^*|_{\tau=0} + o(\tau).$$

If $\tau = 0$, the optimal temperature path to overflow is $h_* = (f_*)^2$, so $\mathcal{I}_{t,\tau}^* = \mathcal{I}_{c^2}(h_*) = \mathcal{I}_c(f_*) = \mathcal{I}_c^*$, and the substitution of $\nabla_\tau G(\tau, f_*^2)|_{\tau=0}$ for $\nabla_\tau I_{t,\tau}^*|_{\tau=0}$ is motivated by an infinite-dimensional version of Danskin's Theorem ([32], Proposition 4.13). To make this rigorous is quite challenging, as the feasible sets in our variational problem depend in a rather intricate way on τ . The explicit calculations for the case $\tau = \tau_0(1, \dots, 1)^T$, $\tau_0 > 0$, are reported in the appendix.

We thus have an approximation of the temperature decay rate which depends only on the current decay rate and the corresponding optimal path. That is, we are able to approximately solve the variational problem for the temperature by solving the one relative to the current, which is generally easier. The capacity region corresponding to the Taylor approximation is

$$\begin{aligned} \tilde{\mathcal{R}}_{\epsilon,p}^{(t,\tau_0,TL)} &:= \{\bar{\mu} \in \mathbb{R}^N : \|\nu\| < 1, \mathcal{I}_{t,\tau}^{(TL)}(\tau, \bar{\mu}) > -\epsilon \log(p)\} = \\ &= \{\bar{\mu} \in \mathbb{R}^N : |\nu_\ell| < 1, \mathcal{I}_c^*(\bar{\mu}) + \tau_0 \Phi_{f_*} > -\epsilon \log(p)\} \end{aligned} \quad (\text{IV.13})$$

In section IV-E we will see that for OU power injections $\mathcal{I}_{t,\tau}^{(TL)} \geq \mathcal{I}_c^*$, and thus $\tilde{\mathcal{R}}_{\epsilon,p}^{(t,\tau,TL)} \supset \tilde{\mathcal{R}}_{\epsilon,p}^{(c)}$. In other words, the capacity region derived via the Taylor expansion is bigger than the one corresponding to the current constraint, as was also the case for the lower bound region. These results confirm the intuition that the temperature-based approach is less conservative than the current-based one. In general, $\tilde{\mathcal{R}}_{\epsilon,p}^{(t,\tau,TL)}$ and $\tilde{\mathcal{R}}_{\epsilon,p}^{(t,\tau,LB)}$ are not subsets of each other. In the following, we compute these capacity regions for OU power injections.

D. Explicit computations for OU: lower bound

In this section we suppose that the power injection process $X^\epsilon(t)$ is the Ornstein-Uhlenbeck process defined in (III.9), and we explicitly compute the lower bound $\mathcal{I}_{t,\tau}^{(LB)}$ and the corresponding

capacity region

$$\tilde{\mathcal{R}}_{\epsilon,p}^{(t,\tau,LB)} := \{\bar{\mu} \in \mathbb{R}^N : \mathcal{I}_{t,\tau}^{(LB)}(\tau, \bar{\mu}) > -\epsilon \log(p)\}.$$

Proposition IV.2. 1) Letting $\alpha_\ell = \sqrt{\frac{1-\nu_\ell^2 e^{-T/\tau_\ell}}{1-e^{-T/\tau_\ell}}}$ and $M_t = L^2 D^{-1}(I - e^{-2Dt})e^{D(t-T)}$, we have that

$$\mathcal{I}_{t,\tau}^{(LB)} = \min_{\ell \in \mathcal{L}'} \frac{(\alpha_\ell - |\nu_\ell|)^2}{C_\ell M_T C_\ell^T},$$

$$\tilde{\mathcal{R}}_{\epsilon,p}^{(t,\tau,LB)} = \bigcap_{\ell \in \mathcal{L}'} \{\bar{\mu} \in \mathbb{R}^N : \frac{(\alpha_\ell - |\nu_\ell|)^2}{C_\ell M_T C_\ell^T} > -\epsilon \log(p)\}.$$

2) In the particular case where $D = \gamma I$ (i.e $\gamma_i = \gamma \forall i$), the capacity region can be rewritten as

$$\tilde{\mathcal{R}}_{\epsilon,p}^{(t,\tau,LB)} := \bigcap_{\ell \in \mathcal{L}'} \{\bar{\mu} \in \mathbb{R}^N : |\nu_\ell| < \delta_\ell\}, \quad (\text{IV.14})$$

where

$$\delta_\ell = \sqrt{1 - \eta_\ell^2 e^{-T/\tau} (1 - e^{-T/\tau})} - \eta_\ell (1 - e^{-T/\tau})$$

$$\in (1 - \eta_\ell, 1),$$

$$\eta_\ell := \sqrt{\frac{\epsilon \log(1/p) \sigma_\ell^2 (1 - e^{-2\gamma T})}{\gamma}} < 1, \quad \sigma_\ell^2 = C_\ell L^2 C_\ell^T.$$

Proof. Thanks to lemma IV.2 we have $\mathcal{I}_{t,\tau}^{(LB)} = \min_{\ell \in \mathcal{L}'} \psi_\ell^{(\alpha_\ell)} \wedge \psi_\ell^{(-\alpha_\ell)}$. From equation (III.10) we get $\psi_\ell^{(\alpha_\ell)} = \frac{(\alpha_\ell - \nu_\ell)^2}{C_\ell M_T C_\ell^T}$ and thus $\psi_\ell^{(\alpha_\ell)} \wedge \psi_\ell^{(-\alpha_\ell)} = \psi_\ell^{(\text{sign}(\nu_\ell)\alpha_\ell)} = \frac{(\alpha_\ell - |\nu_\ell|)^2}{C_\ell M_T C_\ell^T}$, yielding the expression for $\tilde{\mathcal{R}}_{\epsilon,p}^{(t,\tau,LB)}$. Inm the particular case $D = \gamma I$, a straightforward calculation yields the desired result. \square

If $D = \gamma I$, we see from equation IV.14 that $\tilde{\mathcal{R}}_{\epsilon,p}^{(t,\tau,LB)}$ is a convex polyhedron in \mathbb{R}^N , as in the case of the current region. In particular, $\tilde{\mathcal{R}}_{\epsilon,p}^{(t,\tau,LB)}$ is a scaled version of the polyhedron $\tilde{\mathcal{R}}_{\epsilon,p}^{(c)}$.

From (??) we see that $\delta_\ell \xrightarrow{\tau \rightarrow \infty} 1$ and $\delta_\ell \xrightarrow{\tau \rightarrow 0} \eta_\ell$. This means that, as τ increases, the capacity region (IV.14) gets closer to the larger region $\{\bar{\mu} \in \mathbb{R}^N : \|\nu\| < 1\}$, which is the stability region for a deterministic system. On the other hand, as $\tau \rightarrow 0$, the region in (IV.14) boils down to the smaller current-based capacity region given in (III.13).

E. Explicit computations for OU: Taylor approximation

In this section we consider again the OU process $X^{(\epsilon)}$ in (III.9) in the particular case $D = \gamma I$, and we develop the capacity regions based on the Taylor approximation of the temperature decay

rate.

Proposition IV.3. For $\tau = \tau_0(1, \dots, 1)^T$ we have

$$\begin{aligned} \mathcal{I}_{t,\tau}^{(TL)} &= (1 + 2\tau_0\gamma) \mathcal{I}_c^*(\bar{\mu}) + o(\tau) = \\ &= (1 + 2\tau_0\gamma) \min_{\ell \in \mathcal{L}'} \frac{(1 - |\nu_\ell|)^2}{C_\ell M_T C_\ell^T} + o(\tau), \end{aligned} \quad (\text{IV.15})$$

$$\tilde{\mathcal{R}}_{\epsilon,p}^{(t,\tau_0,TL)} = \bigcap_{\ell \in \mathcal{L}'} \left\{ \bar{\mu} \in \mathbb{R}^N : |\nu_\ell| < 1 - \eta_\ell / \sqrt{1 + 2\tau_0\gamma} \right\},$$

where $\eta_\ell := \sqrt{\frac{\epsilon \log(1/p) \sigma_\ell^2 (1 - e^{-2\gamma T})}{\gamma}}$ and $\sigma_\ell^2 = C_\ell L^2 C_\ell^T$.

Proof. In the case $D = \gamma I$, according to equation (III.12), the optimal current paths to overflow in line ℓ and the corresponding decay rate are

$$\begin{aligned} Y^{(\ell)}(t) &= (\text{sign}(\nu_\ell) - \nu_\ell) \frac{(1 - e^{-2\gamma t}) e^{\gamma(t-T)}}{1 - e^{2\gamma T}} R^\ell + \nu, \\ \psi_\ell &= \frac{\gamma}{1 - e^{-2\gamma T}} \frac{(1 - |\nu_\ell|)^2}{\sigma_\ell^2}, \end{aligned} \quad (\text{IV.16})$$

where $R^\ell := \frac{CL^2 C_\ell^T}{C_\ell L^2 C_\ell^T} \in \mathbb{R}^L$ and $\sigma_\ell^2 = C_\ell L^2 C_\ell^T$. Take any $\ell^* \in \arg \min_{\ell \in \mathcal{L}'} \psi_\ell$. Note that, while there may exist multiple indexes ℓ^* that minimize ψ_ℓ , in order to compute the approximation only the value of the achieved minimum $\min_{\ell \in \mathcal{L}'} \psi_\ell$ is needed. Recall also that ℓ^* depends on the initial condition $\bar{\mu}$, i.e. $\ell^* = \ell^*(\bar{\mu})$. Letting $S^* = \text{sign}(\nu_{\ell^*}) - \nu_{\ell^*} \in \mathbb{R}$ and $R^* = R^{\ell^*}$, the optimal current path to overflow is $f_*(t) = Y^{(\ell^*)}(t)$ and in particular $f_*(0) = \nu$, $f_*(T) = S^* R^* + \nu$, $(f_*)'(0) = \frac{2\gamma e^{\gamma T}}{1 - e^{-2\gamma T}} S^* R^*$, $(f_*)'(T) = \frac{\gamma(1 + e^{-2\gamma T})}{1 - e^{-2\gamma T}} S^* R^*$. After a lengthy but straightforward calculation, which can be found in the appendix, the formula for the Taylor approximation reads

$$\mathcal{I}_{t,\tau}^{(TL)}(\bar{\mu}) = (1 + 2\tau_0\gamma) \mathcal{I}_c^*(\bar{\mu}) + o(\tau). \quad (\text{IV.17})$$

The capacity region defined by the Taylor approximation is thus

$$\begin{aligned} \tilde{\mathcal{R}}_{\epsilon,p}^{(t,\tau_0,TL)} &= \bigcap_{\ell \in \mathcal{L}'} \left\{ \bar{\mu} \in \mathbb{R}^N : \right. \\ &\quad \left. \frac{\gamma(1 - |\nu_\ell|)^2}{(1 - e^{-2\gamma T}) \sigma_\ell^2} (1 + 2\tau_0\gamma) > -\epsilon \log(p) \right\}, \end{aligned}$$

which can be rewritten as

$$\tilde{\mathcal{R}}_{\epsilon,p}^{(t,\tau_0,TL)} = \bigcap_{\ell \in \mathcal{L}'} \left\{ \bar{\mu} \in \mathbb{R}^N : |\nu_\ell| < 1 - \eta_\ell / \sqrt{1 + 2\tau_0\gamma} \right\}.$$

□

It is clear that $\tilde{\mathcal{R}}_{\epsilon,p}^{(t,t,\tau_0L)}$ is a convex polyhedron, as it was the case for the current region $\tilde{\mathcal{R}}_{\epsilon,p}^{(c)}$

and the lower bound region $\tilde{\mathcal{R}}_{\epsilon,p}^{(t,\tau_0,LB)}$. Moreover, since $1 + 2\tau_0\gamma > 0$, we immediately get that $\tilde{\mathcal{R}}_{\epsilon,p}^{(t,\tau_0,TL)} \supset \tilde{\mathcal{R}}_{\epsilon,p}^{(c)}$ and that $\tilde{\mathcal{R}}_{\epsilon,p}^{(t,\tau_0,TL)}$ is a re-scaled version of the polyhedron $\tilde{\mathcal{R}}_{\epsilon,p}^{(c)}$. Recall that this was also the case for the lower bound capacity region. The difference is that, while the lower bound holds for every $\tau \in \mathbb{R}^L, \tau > 0$, the expansion $\mathcal{I}_{t,\tau}^{(TL)}$ approximates well the actual decay rate $\mathcal{I}_{t,\tau}^*$ only for small τ_0 (and thermal constant of the form $\tau = \tau_0(1, \dots, 1)^T$). In the numerics section we will see that both the lower bound and the Taylor expansion have their use, as in some cases $\tilde{\mathcal{R}}_{\epsilon,p}^{(t,t,\tau_0L)} \subset \tilde{\mathcal{R}}_{\epsilon,p}^{(t,\tau,LB)}$ and in others $\tilde{\mathcal{R}}_{\epsilon,p}^{(t,t,\tau_0L)} \supset \tilde{\mathcal{R}}_{\epsilon,p}^{(t,\tau,LB)}$, depending on the parameters.

V. NUMERICS

In this section numerical results for the OU case (III.9) with $D = \gamma I$ are reported.

A. 1-dimensional case

For the very simple case of one line and two buses (one of which is the slack bus), i.e. $m = L = 1$, we show how to numerically compute the decay rate $\mathcal{I}_{t,\tau}^*$. A summary of these results has been given without proofs in [12]. We want to minimize, under the constraints $\theta(0) = \mu^2$ and $\theta(1) = 1$, the functional

$$\mathcal{I}(\theta) = \frac{1}{2} \int_0^T \left(\frac{\tau\theta'' + \theta'}{2\sqrt{\tau\theta' + \theta}} + \gamma\sqrt{\tau\theta' + \theta} - \gamma\mu \right)^2 ds.$$

Making the substitution $f = \tau\theta' + \theta$ and applying the Euler criterion, the optimal solution satisfies the third order ordinary differential equation

$$4\gamma^2 f^3 + 2\tau f^2 f''' - 2f^2 f'' + f(f')^2 - 4\tau f f' f'' + 2\tau(f')^3 = 0.$$

which can be rewritten as a 4-dimensional implicit first order system

$$\phi(y, y') = 0, \tag{V.1}$$

where $y = [\theta, f, f', f'']^T$ and

$$\phi(y, y') = \begin{bmatrix} y_2 - \tau y_1' - y_1 \\ y_3 - y_2' \\ y_4 - y_3' \\ 4\gamma^2 y_2^3 + 2\tau y_2^2 y_4' - 2y_2^2 y_4 + y_2 y_3'^2 - 4\tau y_2 y_3 y_4 + 2\tau y_3^3 \end{bmatrix}$$

with $\theta(0) = y_1(0) = \mu^2$ and $f(0) = y_2(0) = \mu^2$.

The solution of (V.1), and hence the optimal value for the original variational problem, is a function of the initial conditions $f'(0) = y_3(0)$ and $f''(0) = y_4(0)$, which are not given. We will denote such function as

$$\mathcal{I}(\theta^*)(x_1, x_2) = \min_{\theta(0)=f(0)=\mu^2, f'(0)=x_1, f''(0)=x_2} \mathcal{I}(\theta).$$

Thus, in order to compute $\mathcal{I}_{t,\tau}^*$, we need to solve an optimization problem where every objective function evaluation involves solving an implicit 4-dimensional system of ordinary differential equations. On the other hand, in the OU case, the computation of the current decay rate \mathcal{I}_c^* and the approximations $\mathcal{I}_{t,\tau}^{(LB)}$, $\mathcal{I}_{t,\tau}^{(TL)}$ incurs no computational cost, since closed-form expressions are available.

Table I reports the values of $\mathcal{I}_{t,\tau}^*$, together with the current rate \mathcal{I}_c^* , the lower bound approximation $\mathcal{I}_{t,\tau}^{(LB)}$ and the Taylor approximation $\mathcal{I}_{t,\tau}^{(TL)}$, for the following choice of parameters: $\mu = 0.5, \gamma = 0.5, l = 1, T = 1, \tau = 0.1, 0.2, 0.3, 0.4, 0.5, 0.6$.

TABLE I: Comparison between the different decay rates.

τ	\mathcal{I}_c^*	$\mathcal{I}_{t,\tau}^{(LB)}$	$\mathcal{I}_{t,\tau}^{(TL)}$	$\mathcal{I}_{t,\tau}^*$
0.6	0.1977	0.2696	0.3164	0.4669
0.5	0.1977	0.2455	0.2966	0.4337
0.4	0.1977	0.2247	0.2768	0.3731
0.3	0.1977	0.2088	0.2571	0.3190
0.2	0.1977	0.1998	0.2373	0.2763
0.1	0.1977	0.1978	0.2175	0.2308

We notice that $\mathcal{I}_c^* \leq \mathcal{I}_{t,\tau}^{(LB)} \leq \mathcal{I}_{t,\tau}^{(TL)} \leq \mathcal{I}_{t,\tau}^*$, which means that the corresponding capacity regions are encapsulated, the current one being the smallest and corresponding to the most conservative approach. In particular, the Taylor approximation constraint is at the same time less conservative than the lower bound and the current constraints, and more conservative than the real temperature constraint. This means that using the Taylor constraint we can afford for larger power injections values than the ones we would have by enforcing the current constraint, while keeping the probability of temperature overload smaller than a fixed value. This one-dimensional example shows that, while the computation of the true temperature decay rate $\mathcal{I}_{t,\tau}^*$ is computationally much more costly than computing the closed-form approximations (which have virtually no cost), for small values of τ the latter perform sufficiently well for our purposes. Using this example as

a guideline, in the multi-dimensional case we will focus only on the current decay rate \mathcal{I}_c^* and the approximations $\mathcal{I}_{t,\tau}^{(LB)}$, $\mathcal{I}_{t,\tau}^{(TL)}$.

B. 3-bus network

In this section we will show the capacity regions for the case of a 3-bus network with 2 stochastic power injections, the slack bus and no deterministic power injections, endowed with a wheel topology. So we have $m = N = 2$, $L = 3$, $\mathcal{N} = 0, 1, 2$ and $\mathcal{L} = \{(0, 1), (0, 2), (1, 2)\}$, as in Figure 2.

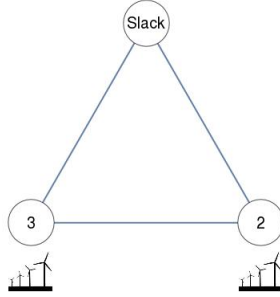


Fig. 2: 3-bus network with 2 stochastic power injections and wheel topology.

We assume $\beta_{ij} = 1$ and $I_{\max,\ell} = 1$ for all $i, j \in \mathcal{N}$, $\ell \in \mathcal{L}$, $l_1 = l_2 = \gamma_1 = \gamma_2 = 1$. In figure 3 the capacity regions are shown for the case $\tau_1 = \tau_2 = 0.5$, $p = 10^{-4}$, $\epsilon = 0.1$ and $T = 1, 0.1$. The bigger external region is the stability region at time $t = 0$, i.e. the region corresponding to a deterministic system

$$\mathcal{R}_{\text{det}} = \{(\mu_1, \mu_2) \in \mathbb{R}^2 \mid |\nu_\ell| < 1 \quad \forall \ell = 1, 2, 3\},$$

with vertical lines is plotted $\tilde{\mathcal{R}}_{\epsilon,p}^{(c)}$, with horizontal lines $\tilde{\mathcal{R}}_{\epsilon,p}^{(t,\tau,LB)}$ and with diagonal lines $\tilde{\mathcal{R}}_{\epsilon,p}^{(t,\tau_0,TL)}$.

The plots clearly show that the regions are convex and polyhedral. Observe that in both cases we have, as expected,

$$\tilde{\mathcal{R}}_{\epsilon,p}^{(c)} \subset \tilde{\mathcal{R}}_{\epsilon,p}^{(t,\tau,LB)}, \tilde{\mathcal{R}}_{\epsilon,p}^{(t,\tau_0,TL)} \subset \tilde{\mathcal{R}}_{\text{det}},$$

(note that, for readability purposes, the overlapping of lines is not shown). In the case $T = 1$, we have $\tilde{\mathcal{R}}_{\epsilon,p}^{(t,\tau,LB)} \subset \tilde{\mathcal{R}}_{\epsilon,p}^{(t,\tau_0,TL)}$, while in the case $T = 0.1$ the reverse inclusion $\tilde{\mathcal{R}}_{\epsilon,p}^{(t,\tau,LB)} \supset \tilde{\mathcal{R}}_{\epsilon,p}^{(t,\tau_0,TL)}$ holds. This shows that for larger T the Taylor approximation is less conservative than the lower bound one, i.e. it better captures the randomness over longer time windows, while for smaller T the situation is reversed. We conclude that both the lower bound region and the Taylor region have their use, depending on the particular parameters.

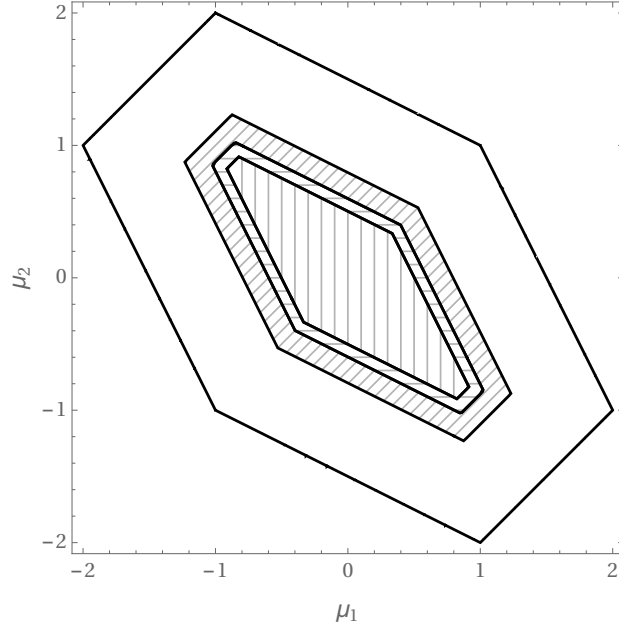
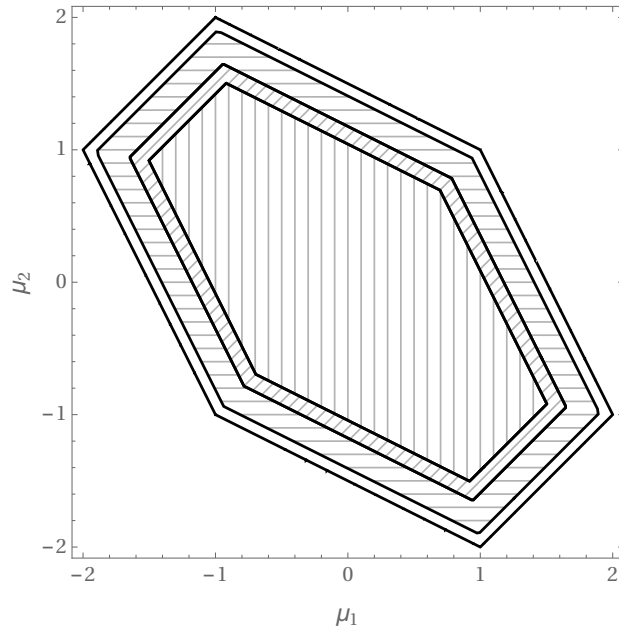
(a) $T = 1$ (b) $T = 0.1$

Fig. 3: Capacity region for the 3-bus network

C. IEEE-14 test network

In this section we develop capacity regions for the IEEE-14 test network, representing a portion of the American Electric Power System [33]. The grid consists of 14 nodes and 20 lines, and the original network has constant and deterministic power injections $P_D \in \mathbb{R}^{14}$. Node 1 is the slack node. We replace two of the deterministic power injections by OU processes with long term mean equal to the original deterministic power injection value, and we keep the other injections deterministic. Furthermore, we assume that we have control over two deterministic power injections, while we keep the others constant and equal to the corresponding values given by P_D . We thus compute two-dimensional capacity regions, which corresponds to the amount of power that can be injected at the two controllable deterministic sources so that the probability of overload during $[0, T]$ is sufficiently small. We extract the values for P_D , β_{ij} , \tilde{C} from the MATPOWER package in MATLAB [34]. The network data assumes the per-unit system. For each line ℓ we set the maximum permissible current $I_{\max, \ell} = K|\tilde{C}_\ell P_D|$ equal to a constant $K > 1$ times the absolute current flowing in that connection in the deterministic setting. We set $K = 1.5$, the final time $T = 1$, the OU parameters equal to $\gamma_i = 1, l_i = 10$, the rarity parameter $\epsilon = 0.25$ and the thermal constant $\tau = 0.5$. We perform two different experiments changing the location of the stochastic nodes.

1) *Stochastic nodes neighbors:* we assume that the nodes that host stochastic power injections are nodes 2 and 3, while the controllable nodes are 6 and 9. The current-based capacity region is

$$\begin{aligned} \tilde{\mathcal{R}}_{\epsilon, p}^{(c)} = \{(\bar{\mu}_6, \bar{\mu}_9) \in \mathbb{R}^2 \mid, \bar{\mu} = (P_{D,2}, \dots, P_{D,5}, \bar{\mu}_6, P_{D,7}, \\ P_{D,8}, \bar{\mu}_9, P_{D,10}, \dots, P_{D,14}), \mathcal{I}_c(\bar{\mu}) \geq -\epsilon \log(p)\}, \end{aligned}$$

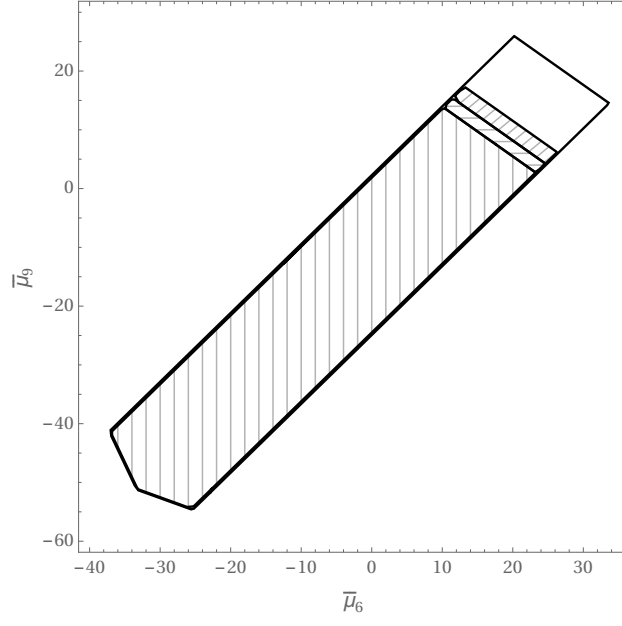
and the other regions are defined similarly. In Figures 4a,4b the 2-dimensional capacity regions $\mathcal{R}_{\text{det}}, \tilde{\mathcal{R}}_{\epsilon, p}^{(c)}, \tilde{\mathcal{R}}_{\epsilon, p}^{(t, \tau, LB)}, \tilde{\mathcal{R}}_{\epsilon, p}^{(t, \tau_0, TL)}$ are shown for two different target probabilities, while in Figure 5a the deterministic region \mathcal{R}_{det} is divided into regions corresponding to the lines at most risk. More precisely, if $\ell^*(\bar{\mu}) := \arg\min_{\ell \in \mathcal{L}} \psi_\ell^{(1)}(\bar{\mu}) \wedge \psi_\ell^{(-1)}(\bar{\mu})$, then the thin sub-region in the north-west part of Figure 5a is

$$S_{(9,10)} := \{(\bar{\mu}_6, \bar{\mu}_9) \in \mathbb{R}^2 \mid \|\nu\| \leq 1, \ell^*(\bar{\mu}) = (9, 10)\},$$

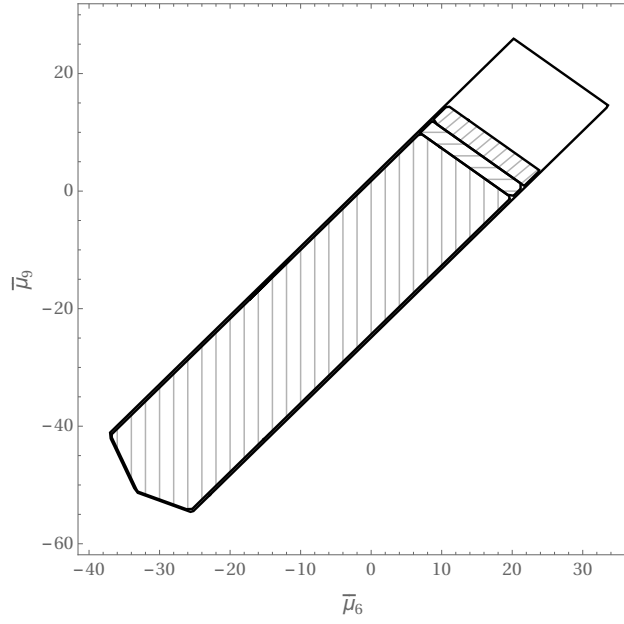
i.e. it consists of power injections at nodes 6 and 9 such that the line with the higher chance of overloading is line (9, 10). Proceeding counterclockwise, the others sub-regions are $S_{(5,6)}$, $S_{(7,9)}$ and $S_{(10,11)}$, and the bigger central region is $S_{(3,4)}$. Finally, in Figure 5b we show the topology of the network: the slack node is vertex 1, the stochastic nodes are represented with square vertexes and the controllable nodes with triangular vertexes. The five lines at most risk are the solid ones.

2) *Stochastic nodes apart:* we now assume that the nodes that host stochastic power injections are nodes 2 and 13, and we keep nodes 6 and 9 as the controllable ones. Figures 7 and 6 show the topology of the network, the capacity regions and their decomposition according to the lines at most risk. In Figure 7a the north-west sub-region is $S_{(9,10)}$, and proceeding counterclockwise the sub-regions are $S_{(5,6)}$, $S_{(4,7)}$, $S_{(10,11)}$ and $S_{(3,4)}$, while the bigger central sub-region is $S_{(12,13)}$.

We notice that reducing the target probability from 10^{-4} to 10^{-7} causes the capacity regions to shrink considerably, in particular the current region $\tilde{\mathcal{R}}_{\epsilon,p}^{(c)}$. In section V-C1 this phenomenon was not as significant. Figure 6b shows that for a target probability of $p = 10^{-7}$ the lower bound region $\tilde{\mathcal{R}}_{\epsilon,p}^{(t,\tau,LB)}$ is more than two times bigger than the current region, and the Taylor region $\tilde{\mathcal{R}}_{\epsilon,p}^{(t,\tau,TL)}$ is approximately two times bigger than $\tilde{\mathcal{R}}_{\epsilon,p}^{(t,\tau,LB)}$. It is thus clear how temperature-based constraints allow for more power injected, with respect to current-based constraints, while keeping the probability of overload below a fixed target.

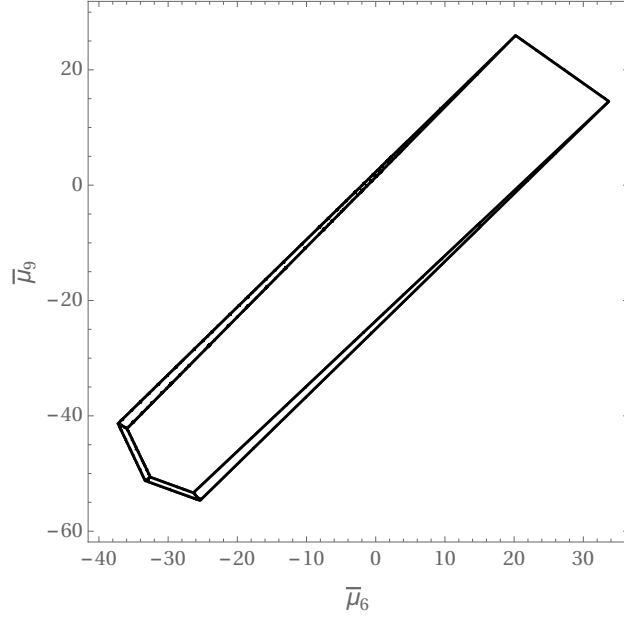


(a) Target probability $p = 10^{-4}$.

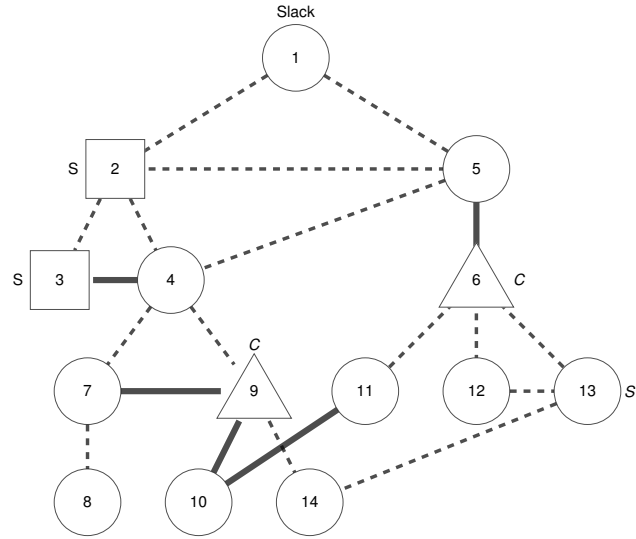


(b) Target probability $p = 10^{-7}$.

Fig. 4: Capacity regions in the case of neighbors stochastic nodes



(a) Subdivision of the deterministic region



(b) Network topology. The lines at most risk are the solid ones

Fig. 5: Lines at most risk in the case of neighbors stochastic nodes

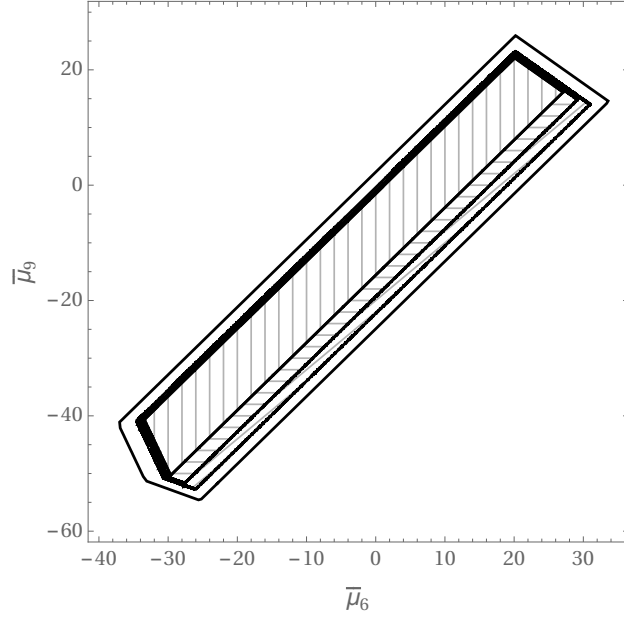
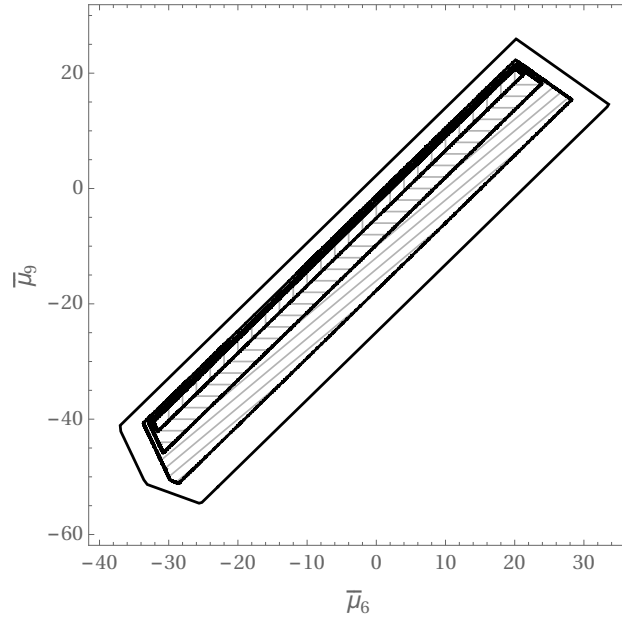
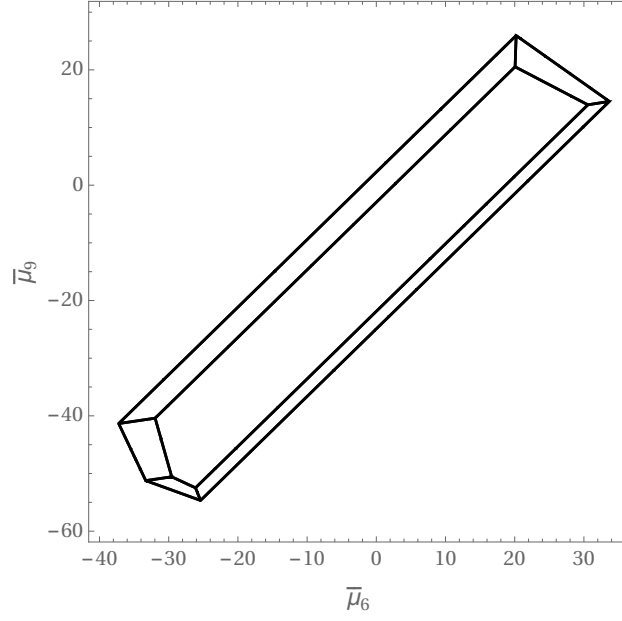
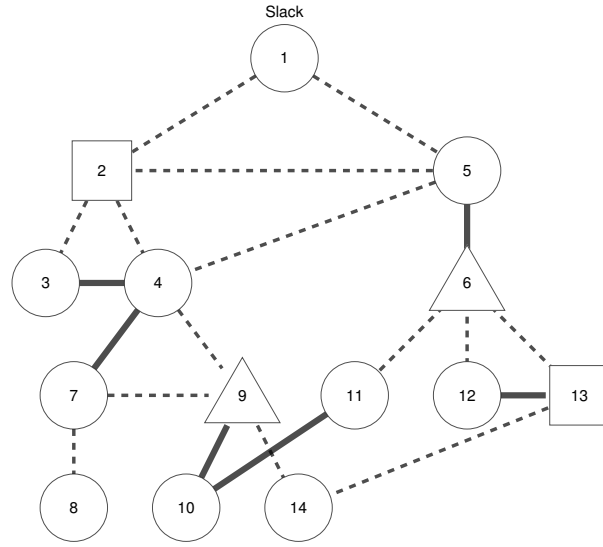
(a) Target probability $p = 10^{-4}$ (b) Target probability $p = 10^{-7}$.

Fig. 6: Capacity regions in the case of stochastic nodes apart



(a) Subdivision of the deterministic region



(b) Network topology

Fig. 7: Lines at most risk in the case of stochastic nodes apart

VI. CONCLUDING REMARKS

We employed large deviations theory to develop tractable capacity regions for power grids with variable power injections, modeled as small-noise diffusion processes, assuming currents behave according to the DC power flow equations. These capacity regions define the set of initial power injections such that the probability of a current/temperature overload in a given interval is very small, and can be used as constraints in OPF formulations. Incorporating the transient relationship between line temperature and line current leads to an enlarged capacity region. While this enlarged region is difficult to compute, we develop tractable approximations of this capacity region that improve upon the capacity region defined by the conservative current overflow constraint.

The potential of our large-deviations result goes beyond the development of capacity regions. Our results can be used to speed up more detailed simulations, in the way recently done in [31]. In addition, the identification of the lines most likely to overload makes our techniques potentially applicable to identify parts of the network that require an extension of the capacity.

In future work, we plan to address several assumptions that play a critical role in our analysis. In particular we plan to consider AC networks and more general classes of input sources, based on hidden Markov models.

VII. PROOFS

Proof of Lemma III.2. Define

$$S_1 = \{g \in H_\mu^1 : \|C_\ell g(t) + y_\ell\|_\infty \geq 1\},$$

$$S_2 = \{g \in H_\mu^1 : |C_\ell g(T) + y_\ell| = 1\}.$$

We have to prove that $\inf_{g \in S_1} \mathcal{I}_p(g) = \inf_{g \in S_2} \mathcal{I}_p(g)$. Since $S_2 \subset S_1$, it follows that $\inf_{g \in S_1} \mathcal{I}_p(g) \leq \inf_{g \in S_2} \mathcal{I}_p(g)$. To prove the reverse inequality, we show that for any $g \in S_1$, there exists $\tilde{g} \in S_2$ such that $\mathcal{I}_p(\tilde{g}) \leq \mathcal{I}_p(g)$. Pick $g \in S_1$. Let $t' \in [0, T]$ be the first time such that $|y_\ell + C_\ell g(t')| = 1$. Clearly $t' > 0$, since $|y_\ell + C_\ell g(0)| = |\nu_\ell| < 1$. If $t' = T$, we may take $\tilde{g}(t) = g(t)$. If $t' < T$, define $\tilde{g}(t)$ by time-shifting $g(t)$ to the right as follows:

$$\tilde{g}(t) = \begin{cases} \mu & \text{for } 0 \leq t < T - t', \\ g(t - T + t') & \text{for } T - t' \leq t \leq T. \end{cases}$$

It is easy to check that $\tilde{g} \in S_2$, and that $\mathcal{I}_p(\tilde{g}) \leq \mathcal{I}_p(g)$, because the path \tilde{g} incurs no cost up to time $T - t'$. Indeed, since in the interval $[0, T - t']$ \tilde{g} is constantly equal to μ , we have $b(\tilde{g}(t)) = b(\mu) = 0$ and $\tilde{g}'(t) = 0$, yielding $\int_0^{T-t'} \left(\frac{g'_i - b_i(g_i)}{l_i(g_i)} \right)^2 dt = 0$ and thus

$$\begin{aligned} \mathcal{I}_p(\tilde{g}) &= \int_0^T \left(\frac{\tilde{g}'_i - b_i(\tilde{g}_i)}{l_i(\tilde{g}_i)} \right)^2 dt = \int_{T-t'}^T \left(\frac{\tilde{g}'_i - b_i(\tilde{g}_i)}{l_i(\tilde{g}_i)} \right)^2 dt = \\ &= \int_0^{t'} \left(\frac{g'_i - b_i(g_i)}{l_i(g_i)} \right)^2 dt \leq \mathcal{I}_p(g). \end{aligned}$$

□

Proof of Lemma III.3. First suppose $a \geq \tilde{a} > \nu_\ell \geq 0$. The case $a \leq \tilde{a} < \nu_\ell \leq 0$ is analogous. We want to show that for all $f \in y + CH_\mu^1$ such that $f_\ell(T) = a$, there exist a $\tilde{f} \in y + CH_\mu^1$ with $\tilde{f}_\ell(T) = \tilde{a}$ and $\mathcal{I}_c(\tilde{f}) \leq \mathcal{I}_c(f)$. Since $f_\ell(0) = \nu_\ell < \tilde{a} \leq a$ and f is continuous, there exist a $t' \in (0, T)$ such that $f(t') = \tilde{a}$. Define $\tilde{f}(t)$ as follows:

$$\tilde{f}(t) = \begin{cases} \nu & \text{for } 0 \leq t < T - t' \\ f(t - T + t') & \text{for } T - t' \leq t \leq T \end{cases}$$

It is easy to check that $\tilde{f} \in y + CH_\mu^1$, $\tilde{f}_\ell(T) = \tilde{a}$ and $\mathcal{I}_c(\tilde{f}) \leq \mathcal{I}_c(f)$. The proof that $\psi_\ell^{(a)}$ is non-increasing for $a < \nu_\ell$ goes along the same lines. □

Proof of Lemma IV.1. The proof goes along the lines of the proof of lemma III.1. First notice that a vector (μ, μ_D) such that $\|\nu\| = \|C\mu + C_D\mu_D\| < 1$ is admissible if and only if the following implication holds:

$$\exists g \in H_\mu^1 \text{ s.t. } \mathcal{I}_p(g) < \epsilon \log(1/p) \implies \|h^{g, \mu, \mu_D}\|_\infty < 1, \quad (\text{VII.1})$$

where

$$\begin{aligned} h_\ell^{g, \mu, \mu_D}(t) &:= \xi_\tau(y + Cg) = (y_\ell + C_\ell \mu)^2 e^{-t/\tau} + \\ &\frac{1}{\tau} \int_0^t e^{-(t-s)/\tau} (y_\ell + C_\ell g(s))^2 ds, \quad y = C_D \mu_D. \end{aligned}$$

For all $\ell \in \mathcal{L}$ and for all $t \in [0, T]$, $h_\ell^{g, \mu, \mu_D}(t)$ is non-negative and convex in μ_D . Using the property (VII.1), the thesis follows. □

Proof of lemma IV.2. The proof follows easily from the observation that the event $\|\Theta_\ell^{\epsilon, \tau}\| \geq 1$ implies the event $\|Y_\ell^\epsilon\| \geq \alpha_\ell$. Indeed, it is easy to check that if $|Y_\ell^\epsilon(t)| < \alpha_\ell$ for all $t \in [0, T]$,

then it follow from (II.6) that $\Theta_\ell^{\epsilon,\tau}(t) < 1$ for all $t \in [0, 1]$. Thus, we have

$$\begin{aligned}
\omega_\ell &= \lim_{\epsilon \downarrow 0} -\epsilon \log P(\|\Theta_\ell^{\epsilon,\tau}\| \geq 1) \\
&\geq \lim_{\epsilon \downarrow 0} -\epsilon \log P(\|Y_\ell^\epsilon\| \geq \alpha_\ell) \\
&= \inf_{g: \|y_\ell + C_\ell g\| \geq \alpha_\ell} \mathcal{I}_p(g) \\
&= \inf_{g: |y_\ell + C_\ell g(T)| = \alpha_\ell} \mathcal{I}_p(g) = \psi_\ell^{(\alpha_\ell)} \wedge \psi_\ell^{(-\alpha_\ell)}.
\end{aligned}$$

□

APPENDIX A

Lemma A.1. *If A is the oriented incidence matrix of a connected graph with $N + 1$ vertices and L edges, then $\text{rank } A = N$ and $\text{Ker}(A) = \text{Span}((1, \dots, 1)^T)$.*

Proof. See lemma 2.2, [35].

□

Proof of Lemma II.2. Since $D_{ll} \neq 0$ for all $l = 1, \dots, L$ we have $\text{rank } D = L$, and by Lemma II.1 we get $\text{rank } \check{B} = N$. Besides, Lemma A.1 guarantees that also $\text{rank } A = N$ and that $\text{Ker}(A) = \text{Span}((1, \dots, 1)^T)$. Since D is nonsingular, $\text{rank}(DA\check{B}) = \text{rank}(A\check{B})$, and clearly $\text{rank}(A\check{B}) \leq \min(\text{rank}(A), \text{rank}(\check{B})) = N$. On the other hand, let $x \in \text{Ker}(A\check{B})$. We have $A\check{B}x = 0 \iff \check{B}x \in \text{Ker}(A) = \text{Span}((1, \dots, 1)^T) \iff \check{B}x = 0 \iff x \in \text{Ker}(\check{B})$, where in the second implication we used that the first component of $\check{B}x$ is 0 due to the structure of \check{B} . Therefore $\text{Ker}(A\check{B}) = \text{Ker}(\check{B})$ has dimension 1 (being $\text{rank } \check{B} = N$) yielding that, due to the rank-nullity theorem, $\text{rank}(A\check{B}) = N + 1 - \dim \text{Ker}(A\check{B}) = N + 1 - 1 = N$. The matrix \bar{C} must thus have N linear independent columns, and observe that since the first column of \check{B} is zero, also the first column of \tilde{C} and \bar{C} is zero. Therefore it must be the case that the columns from 2 to $N + 1$ of \bar{C} are linearly independent, yielding that also the columns from 2 to $m \leq N$ are, i.e. the matrix C has full rank m .

□

Proof of equation (IV.11). Write the current squared rate given in (IV.8) as

$$\mathcal{I}_{c^2}(F) = \sum_{i=1}^m \int_0^T K_i(F(t), F'(t)) dt, \quad (\text{A.1})$$

where

$$K_i(F(t), F'(t)) = \left[\frac{C_i^+ f'_F(t) - b_i(C_i^+(f_F(t) - y))}{l_i(C_i^+(f_F(t) - y))} \right]^2$$

The partial derivatives of the function $\tau \rightarrow K_i((\tau h' + h), (\tau h'' + h'))$ in $\tau = 0$ read

$$\begin{aligned} & \frac{\partial}{\partial \tau_\ell} K_i(\tau h' + h, \tau h'' + h') \Big|_{\tau=0} \\ &= K_i^{(\ell)}(h, h') h'_\ell + K_i^{(L+\ell)}(h, h') h''_\ell, \end{aligned}$$

thus

$$\sum_{\ell=1}^L \frac{\partial}{\partial \tau_\ell} K_i(\tau h' + h, \tau h'' + h') \Big|_{\tau=0} = \frac{d}{dt} K_i(h, h')$$

and

$$\begin{aligned} & \sum_{\ell=1}^L \frac{\partial}{\partial \tau_\ell} G_h(\tau, \mu) \Big|_{\tau=0} = \sum_{\ell=1}^L \frac{\partial}{\partial \tau_\ell} \mathcal{I}_{c^2}(\tau_\ell h' + h) \Big|_{\tau=0} \\ &= \sum_{\ell=1}^L \sum_{i=1}^m \int_0^T \frac{\partial}{\partial \tau_\ell} K_i(\tau h' + h, \tau h'' + h') \Big|_{\tau=0} \\ &= \sum_{i=1}^m \int_0^T \sum_{\ell=1}^L \frac{\partial}{\partial \tau_\ell} K_i(\tau h' + h, \tau h'' + h') \Big|_{\tau=0} \\ &= \sum_{i=1}^m \int_0^T \frac{d}{dt} K_i(h, h') dt = \sum_{i=1}^m \left[K_i(h(T), h'(T)) - \right. \\ & \quad \left. K_i(h(0), h'(0)) \right] =: \Phi(f_h(0), f_h(T), f_{h'}(0), f_{h'}(T)) =: \Phi_{f_h}. \end{aligned}$$

If $\tau = \tau_0(1, \dots, 1)^T$, $\tau_0 > 0$, we thus get $\tau \cdot \nabla G_h(\tau, \mu) \Big|_{\tau=0} = \tau_0 \Phi_{f_h}$. Finally, formula (IV.10) follows by noticing that if f_* is the optimal current path and $h_* = (f_*)^2$ then $f_{h_*} = f_*$. \square

Proof of equation (IV.15). We have

$$\begin{aligned}
K_i(h_*(T), (h_*)'(T)) &= H_i(C_i^+(f_*(T) - y), C_i^+ f'_*(T)) \\
&= \frac{1}{2l_i^2} \left(C_i^+ f'_*(T) + \gamma C_i^+(f_*(T) - y) - \gamma \mu_i \right)^2 \\
&= \frac{1}{2l_i^2} \left(\frac{\gamma(1 + e^{-2\gamma T})}{1 - e^{-2\gamma T}} S^* C_i^+ R + \gamma(C_i^+ S^* R^* + C_i^+(\nu - y)) - \gamma \mu_i \right)^2 \\
&= \frac{\left(\gamma(1 + e^{-2\gamma T}) S^* C_i^+ R^* + (1 - e^{-2\gamma T}) \gamma(C_i^+ S^* R^*) \right)^2}{2l_i^2(1 - e^{-2\gamma T})^2} \\
&= \frac{2\gamma^2(1 - |\nu_{\ell^*}|)^2}{l_i^2(1 - e^{-2\gamma T})^2} \left(C_i^+ R^* \right)^2; \\
K_i(h_*(0), (h_*)'(0)) &= H_i(C_i^+(f_*(0) - y), C_i^+ f'_*(0)) \\
&= \frac{1}{2l_i^2} \left(C_i^+ f'_*(0) + \gamma C_i^+(f_*(0) - y) - \gamma \mu_i \right)^2 \\
&= \frac{1}{2l_i^2} \left(\frac{2\gamma e^{-\gamma T}}{1 - e^{-2\gamma T}} S^* C_i^+ R^* + \gamma C_i^+(\nu - y) - \gamma \mu_i \right)^2 \\
&= \frac{2\gamma^2 e^{-2\gamma T}(1 - |\nu_{\ell^*}|)^2}{l_i^2(1 - e^{-2\gamma T})^2} \left(C_i^+ R^* \right)^2; \\
\Phi_{f_*} &= \sum_{i=1}^m \left[K_i(h_*(T), (h_*)'(T)) - K_i(h_*(0), (f'_*)'(0)) \right] \\
&= \frac{2\gamma^2(1 - |\nu_{\ell^*}|)^2}{1 - e^{-2\gamma t}} \sum_{i=1}^m \left(\frac{C_i^+ R^*}{l_i} \right)^2.
\end{aligned}$$

The Taylor approximation thus reads

$$\begin{aligned}
\mathcal{I}_{t,\tau}^{(TL)}(\tau_0, \bar{\mu}) &:= \mathcal{I}_c^*(\bar{\mu}) + \tau_0 \Phi_h = \\
&= \frac{\gamma}{1 - e^{-2\gamma T}} \frac{(1 - |\nu_{\ell^*}|)^2}{\sigma_{\ell^*}^2} + \frac{2\tau_0 \gamma^2 (1 - |\nu_{\ell^*}|)^2}{1 - e^{-2\gamma t}} \sum_{i=1}^m \left(\frac{C_i^+ R^*}{l_i} \right)^2 = \\
&= \frac{\gamma(1 - |\nu_{\ell^*}|)^2}{1 - e^{-2\gamma T}} \left(\frac{1}{\sigma_{\ell^*}^2} + 2\tau_0 \gamma \sum_{i=1}^m \left(\frac{C_i^+ R^*}{l_i} \right)^2 \right) = \\
&= \frac{\gamma(1 - |\nu_{\ell^*}|)^2}{(1 - e^{-2\gamma T}) \sigma_{\ell^*}^2} \left(1 + 2\tau_0 \gamma \sum_{i=1}^m \left(\frac{C_i^+ R^*}{l_i} \right)^2 \sigma_{\ell^*}^2 \right) = \\
&= \frac{\gamma(1 - |\nu_{\ell^*}|)^2}{(1 - e^{-2\gamma T}) \sigma_{\ell^*}^2} \left(1 + 2\tau_0 \gamma \sum_{i=1}^m \frac{l_i^2 C_{\ell^* i}^2}{\sigma_{\ell^*}^2} \right) = \\
&= \frac{\gamma(1 - |\nu_{\ell^*}|)^2}{(1 - e^{-2\gamma T}) \sigma_{\ell^*}^2} \left(1 + 2\tau_0 \gamma \right) = (1 + 2\tau_0 \gamma) \mathcal{I}_c^*(\bar{\mu}).
\end{aligned}$$

□

REFERENCES

- [1] Y. Yang, “Hybrid grids,” *DNV GL Strategic research innovation position paper 2*, 2015.

- [2] E. Ela, M. Milligan, and B. Kirby, "Operating reserves and variable generation," National Renewable Energy Laboratory, Tech. Rep., 2011.
- [3] A. Mills and R. Wiser, "Implications of wide-area geographic diversity for short-term variability of solar power," Lawrence Berkeley National Laboratory, Tech. Rep., 2010.
- [4] B. Hodge, S. Shedd, and A. Florita, "Examining the variability of wind power output in the regulation time frame," National Renewable Energy Laboratory, Tech. Rep., 2012.
- [5] W. Fu and J. McCalley, "Risk based optimal power flow," in *Proceedings of IEEE Porto Power Tech Conference*, 2001.
- [6] W. Wadman, D. Crommelin, and J. Frank, "Applying a splitting technique to estimate electrical grid reliability," in *Proceedings of the Winter Simulation Conference*, 2013.
- [7] W. Wadman, G. Bloemhof, D. Crommelin, and J. Frank, "Probabilistic power flow simulation allowing temporary current overloading," in *Proceedings of the International Conference on Probabilistic Methods Applied to Power Systems*, 2012.
- [8] J. F. Shortle, "Efficient simulation of blackout probabilities using splitting," *International Journal of Electrical Power & Energy Systems*, vol. 44, no. 1, pp. 743 – 751, 2013.
- [9] L. Powell, *Power system load flow analysis*. McGraw Hill Professional, 2004.
- [10] A. J. Wood and B. F. Wollenberg, *Power generation, operation, and control*. John Wiley & Sons, 2012.
- [11] A. Dembo and O. Zeitouni, *Large deviations techniques and applications*. Springer, 1998.
- [12] J. Bosman, J. Nair, and B. Zwart, "On the probability of current and temperature overloading in power grids: a large deviations approach," *ACM SIGMETRICS Performance Evaluation Review*, vol. 42, no. 2, pp. 33–35, 2014.
- [13] H. Wan, J. McCalley, and V. Vittal, "Increasing thermal rating by risk analysis," *IEEE Transactions on Power Systems*, vol. 14, no. 3, pp. 815–828, 1999.
- [14] T. R. US-Canada Power System Outage Task Force, "Final report on the august 14, 2003 blackout in the united states and canada," Tech. Rep., 2004.
- [15] FERC and T. R. NERC, "Arizona-southern california outages on september 8, 2011," Tech. Rep., 2012.
- [16] D. Phan and S. Ghosh, "Two-stage stochastic optimization for optimal power flow under renewable generation uncertainty," *ACM Transactions on Modeling and Computer Simulation*, vol. 24, no. 1, 2014.
- [17] T. Summers, J. Warrington, M. Morari, and J. Lygeros, "Stochastic optimal power flow based on convex approximations of chance constraints," 2014, under submission.
- [18] D. Bienstock, J. Blanchet, and J. Li, "Stochastic models and control for electrical power line temperature," *Energy Systems*, pp. 1–20.
- [19] D. Bienstock, M. Chertkov, and S. Harnett, "Chance-constrained optimal power flow: Risk-aware network control under uncertainty," *SIAM Review*, vol. 56, no. 3, pp. 461–495, 2014.
- [20] N. Li, L. Chen, and S. Low, "Optimal demand response based on utility maximization in power networks," in *IEEE Power and Energy Society General Meeting*, 2011.
- [21] S. Madaeni and R. Sioshansi, "The impacts of stochastic programming and demand response on wind integration," *Energy Systems*, vol. 4, no. 2, pp. 109–124, 2013.
- [22] J. Barton and D. Infield, "Energy storage and its use with intermittent renewable energy," *IEEE Transactions on Energy Conversion*, vol. 19, no. 2, pp. 441–448, 2004.
- [23] J. H. Kim and W. B. Powell, "Optimal energy commitments with storage and intermittent supply," *Operations Research*, vol. 59, no. 6, pp. 1347–1360, 2011.
- [24] C. Weber, "Adequate intraday market design to enable the integration of wind energy into the european power systems," *Energy Policy*, vol. 38, no. 7, pp. 3155–3163, 2010.

- [25] J. Nair, S. Adlakha, and A. Wierman, “Energy procurement strategies in the presence of intermittent sources,” in *Proceedings of ACM SIGMETRICS*, 2014.
- [26] B. Stott, J. Jardim, and O. Alsac, “Dc power flow revisited,” *IEEE Transactions on Power Systems*, vol. 24, no. 3, pp. 1290–1300, 2009.
- [27] S. Iwamoto and Y. Tamura, “A load flow calculation method for ill-conditioned power systems,” *IEEE Transactions on Power Apparatus and Systems*, vol. 100, no. 4, pp. 1736–1743, 1981.
- [28] J. Baillieul and C. I. Byrnes, “Geometric critical point analysis of lossless power system models,” *IEEE Transactions on Circuits and Systems*, vol. 29, no. 11, pp. 724–737, 1982.
- [29] D. K. Molzahn, B. C. Lesieutre, and C. L. DeMarco, “A sufficient condition for power flow insolvability with applications to voltage stability margins,” *IEEE Transactions on Power Systems*, vol. 28, no. 3, pp. 2592–2601, 2013.
- [30] H. Pender and W. Del Mar, *Electrical engineers’ handbook*. Wiley, 1949.
- [31] W. S. Wadman, D. T. Crommelin, and B. P. Zwart, “A large deviation based splitting estimation of power flow reliability,” to appear in *ACM-TOMACS*, 2016.
- [32] J. F. Bonnans and A. Shapiro, *Perturbation analysis of optimization problems*. Springer, 2000.
- [33] R. D. Christie. (2006) Power systems test case archive. [Online]. Available: <http://www.ee.washington.edu/research/pstca/>
- [34] R. D. Zimmerman, C. E. Murillo-Sánchez, and R. J. Thomas, “Matpower: Steady-state operations, planning, and analysis tools for power systems research and education,” *Power Systems, IEEE Transactions on*, vol. 26, no. 1, pp. 12–19, 2011.
- [35] R. B. Bapat, *Graphs and matrices*. Springer, 2010.



Tommaso Nesti received his B.Sc and M.Sc degree in Mathematics from University of Pisa, Italy (2015). From 2015 he is a Ph.D student in the Stochastic group at Centrum Wiskunde & Informatica (CWI) in Amsterdam. His research interests are in the area of applied probability and numerical analysis, focusing on problems arising in the study of energy and queueing networks. His current research is on rare-event and reliability analysis of energy networks under uncertainty.



Jayakrishnan Nair received his BTech and MTech in Electrical Engg. (EE) from IIT Bombay (2007) and Ph.D. in EE from California Inst. of Tech. (2012). He has held post-doctoral positions at California Inst. of Tech. and Centrum Wiskunde & Informatica. He is currently an Assistant Professor in EE at IIT Bombay. His research focuses on modeling, performance evaluation, and design issues in queueing systems and communication networks. His recent interests include game theoretic interactions in queueing systems and smart power grids.



Bert Zwart is a researcher at the Center for Mathematics and Computer Science (CWI) in Amsterdam, where he leads the Stochastic group. He also holds secondary professorial positions at Eindhoven University of Technology. His research is in applied probability, inspired by problems in computer, communication, energy and service networks. Zwart is the 2008 recipient of the Erlang prize, an IBM faculty award, VENI, VIDI and VICI awards from the Dutch Science Foundation NWO, the 2015 Van Dantzig Prize, and 4 best papers awards. Zwart has been area editor of Stochastic Models for the journal Operations Research since 2009, and serves on several additional journal boards and program committees.